

# Adipocyte-Specific Deletion of Sine Oculis Homeobox Homolog 1 Inhibits Lipolysis and Reduces Skin Fibrosis

Nancy Wareing<sup>1,2</sup>, Tingting W Mills<sup>1</sup>, Scott Collum<sup>1</sup>, Minghua Wu<sup>2</sup>, Lucy Revercomb<sup>3</sup>, Rene Girard<sup>1</sup>, Hui Liu<sup>1</sup>, Alexes Daquinag<sup>4</sup>, Mikhail Kolonin<sup>4</sup>, Marka Lyons<sup>2</sup>, Brian Skaug<sup>2</sup>, Weizhen Bi<sup>1</sup>, Meer A. Ali<sup>5</sup>, Haniyeh Koochak<sup>6</sup>, Anthony R Flores<sup>6</sup>, Yuntao Yang<sup>5</sup>, W Jim Zheng<sup>5</sup>, William R Swindell<sup>7</sup>, Shervin Assassi<sup>2\*</sup>, Harry Karmouty-Quintana<sup>1,8\*</sup>

<sup>1</sup> Department of Biochemistry and Molecular Biology, McGovern Medical School, University of Texas Health Science Center at Houston (UTHealth Houston), TX, USA; <sup>2</sup> Division of Rheumatology, Department of Internal Medicine, McGovern Medical School, UTHealth Houston, Houston TX, USA; <sup>3</sup> Rice University, Houston TX, USA, <sup>4</sup> Center for Metabolic and Degenerative Diseases, Institute of Molecular Medicine, UTHealth Houston, Houston TX, USA, <sup>5</sup> D Bradley McWilliams School of Biomedical Informatics, Department of Internal Medicine, McGovern Medical School, UTHealth Houston, Houston TX, USA; <sup>6</sup> Department of Pediatrics, McGovern Medical School, UTHealth Houston, Houston TX, USA, <sup>7</sup> Department of Internal Medicine, University of Texas Southwestern Medical Center, Dallas, TX; <sup>8</sup> Division of Pulmonary, Critical Care, and Sleep Medicine, Department of Internal Medicine, McGovern Medical School, UTHealth Houston, Houston TX, USA

The University of Texas Health Science Center at Houston

\*Co-corresponding authors

Corresponding Authors:

Shervin Assassi M.D., M.S.

6431 Fannin Street, Suite 5.260, Houston, TX 77030

Phone: 713 500 6888

Fax: 713 512 2246

Email: Shervin.Assassi@uth.tmc.edu

Harry Karmouty-Quintana, Ph.D.

6431 Fannin Street, Suite 6.214, Houston, TX 77030

Phone: 713 500 5331

Email: Harry.Karmouty@uth.tmc.edu

38 **Abstract**

39 Dermal fibrosis is a cardinal feature of systemic sclerosis (SSc) for which there are limited  
40 Systemic sclerosis (SSc) is characterized by dermal fibrosis accompanied by loss of  
41 dermal white adipose tissue (DWAT), yet the mechanisms linking adipocyte depletion to  
42 fibroblast activation remain unclear. Here we identify the transcription factor SIX1 as a  
43 central regulator coupling adipogenic repression with profibrotic signaling. SIX1  
44 expression was increased in skin biopsies from two independent SSc cohorts and  
45 localized to fibroblast and perivascular stromal cells. In mice, ubiquitous or adipocyte-  
46 specific deletion of *Six1* preserved DWAT, reduced collagen accumulation, and  
47 selectively decreased pro-fibrotic mediators. In cultured fibroblasts, CRISPR/Cas9-  
48 mediated *Six1* loss enhanced adipogenic markers while reducing profibrotic mediators  
49 and directly suppressed PAI-1 (*SERPINE1*) promoter activity. Together, these data  
50 position SIX1 as a transcriptional switch that promotes adipocyte reprogramming and  
51 fibrotic progression, and highlight SIX1 inhibition as a potential therapeutic strategy to  
52 preserve adipocyte identity and limit dermal fibrosis.

53

54 Keywords: systemic sclerosis, scleroderma, fibrosis, adipose

55

56

57 **Short Summary:**

58 **SIX1 is elevated in systemic sclerosis skin and linked to adipose-associated**  
59 **biology. Deleting SIX1 in adipocytes reduces fibrosis, making it a potential**  
60 **therapeutic target.**

61

62

## 63 **Introduction**

64 Systemic sclerosis (SSc; or scleroderma) is a rare and heterogeneous autoimmune  
65 connective tissue disorder.(1, 2) The multiorgan dysfunction has been characterized as  
66 a triad of immune dysregulation, vasculopathy, and excessive extracellular matrix (ECM)  
67 deposition by myofibroblasts, leading to skin and internal organ fibrosis.(2-4) Skin  
68 thickening and tightening is responsible for considerable morbidity in this debilitating  
69 disease.(5, 6) The extent of skin fibrosis defines the two subclasses of SSc: limited  
70 cutaneous (lcSSc) and diffuse cutaneous SSc (dcSSc).(3) There are currently no FDA-  
71 approved treatments for skin involvement in SSc. More extensive skin involvement at the  
72 time of diagnosis is associated with higher levels of disability, severity of pain, and  
73 decreased survival.(7, 8) This underscores the urgent need to identify novel targeted  
74 therapies for the treatment of SSc.(9)

75

76 Thus, understanding the early pathogenesis of disease represents a critical step towards  
77 novel therapeutic approaches.(9) The mechanisms that lead to organ fibrosis in SSc are  
78 not fully understood; however, similar mediators have been identified to play a role in the  
79 lung and skin. For example, increased adenosine, hyaluronan, and IL-6 have been  
80 implicated in the pathophysiology of both lung and skin fibrosis(10-14). However, these  
81 mechanisms have largely focused on fibroblast and epithelial biology, with limited studies  
82 in adipocytes. This is important as an early hallmark of SSc is skin-associated adipose  
83 tissue atrophy and replacement by extracellular matrix, leading to dermal thickening.(15,  
84 16) Clinically, this may directly contribute to rigidity and tethering observed in early  
85 lesional SSc skin (15, 16). Dermal white adipocyte tissue (DWAT) adipocytes display

86 highly distinct features compared to other white adipocytes, including significant  
87 plasticity(17-19). They can cycle through de-differentiation and re-differentiation as part  
88 of a physiologic response to hair cycling, aging, and energy demands.(17, 18, 20) Under  
89 certain conditions, de-differentiated pre-adipocytes escape the normal cycle of  
90 redifferentiation and *trans*-differentiate into ECM-producing myofibroblasts. This process  
91 is referred to as the adipocyte-to-myofibroblast transition (AMT).(21, 22) AMT has been  
92 well-studied in wound healing (21, 23) and recent evidence suggests it may also  
93 contribute to pathological skin fibrosis.(22, 24) Mature adipocytes in the skin produce  
94 PDGF ligands and BMPs, both of which are implicated in wound healing and fibrosis. (25)  
95 In addition, the adipose secretome has also been identified to play a role in the  
96 pathophysiology of SSc. (26) Lipid-filled adipocytes cross-talk with other cell types in the  
97 stroma-vascular fraction of adipose tissue. The interaction between the dermal fibroblasts  
98 and adipocytes has also been appreciated as a contributor to irregular inflammation and  
99 aberrant wound healing through pro-inflammatory signaling between cell types (27) and  
100 adipocyte-driven regulation of fibroblast ECM production. (28) A robust physiologic axis  
101 also exists between adipocytes and endothelial cells, by which cell signaling can be  
102 bidirectionally regulated. (29) However, mechanisms by which adipocytes contribute to  
103 the pathogenesis of skin fibrosis in SSc remain poorly understood.

104

105 Our group and others identified sine oculis homeobox homolog 1 (SIX1) as a novel  
106 mediator in lung fibrosis, promoting the release of pro-fibrotic mediators by alveolar  
107 epithelial cells.(30-32) Further, SIX1 has also been implicated in asthmatic lung fibrosis  
108 (31, 32) and in liver fibrosis defined by excessive myofibroblast activation and ECM

109 deposition (33). Lung fibrosis is an important complication of SSc that is typically  
110 observed following onset of skin fibrosis, and while epithelial and fibroblast-based  
111 mechanisms are most highly studied, the contribution of the adipocyte to the fibrotic  
112 process is not fully known.(34) However, whether SIX1 plays a role in skin fibrosis in SSc  
113 is not known; in particular, how adipocyte SIX1 regulates dermal fibrosis remains under  
114 investigated. SIX1 is a member of an evolutionarily conserved family of developmental  
115 transcription factors.(35) SIX1 plays a critical role in regulating the expression of genes  
116 that control precursor cell survival and proliferation during embryogenesis. In healthy  
117 adults, SIX1 is negligibly expressed in most tissues.(36) Perhaps the most well-studied  
118 role of SIX1 in adulthood is in the context of cancer, where it is a critical regulator of trans-  
119 differentiation of pre-cancerous cells into mesenchymal cells with metastatic features.(37-  
120 41) Although *SIX1* transcript expression has been identified in healthy subcutaneous  
121 adipose tissue(42), to date its exact role in adipose tissue biology remains poorly  
122 investigated. Brunmeir et al.(43) were the first to identify the direct transcription regulation  
123 by SIX1 and the interaction between SIX1 and major regulators of adipogenesis, in  
124 mature fat cells. Recently, it was demonstrated that *in vivo* SIX1 overexpression in mouse  
125 hepatocytes exacerbates diet-induced liver inflammation, metabolic disruption, and  
126 hepatic steatosis, and activates liver-specific receptors to induce de novo lipogenesis.(44)  
127 This work is founded upon the fundamental and newly developing understanding of the  
128 roles of SIX1, particularly in the realm of lipolysis and the release of pro-fibrotic factors  
129 that regulate dermal fibrosis. We hypothesize that SIX1 contributes to dermal lipoatrophy  
130 and skin fibrosis in SSc. Surprisingly, our data suggests that SIX1 is not involved in

131 modulating adipocyte phenotype, but instead it regulates the release of the pro-fibrotic  
132 mediator, PAI-1 that promotes dermal fibrosis.

133

134

135 **Results**

136 **Increased *SIX1* levels correlate to skin fibrosis in SSc patients.**

137  
138 Previously, our group identified increased *SIX1* in lung fibrosis(30) and *SIX1* expression  
139 has been identified to be present in subcutaneous adipocytes, particularly in those  
140 exhibiting aberrant function (42). As such we aimed to determine whether *SIX1* was  
141 elevated in skin samples from SSc patients. To do this, we first determined expression of  
142 *SIX1* from two distinct cohorts: The GENISOS (Genetics versus ENvironment In  
143 Scleroderma Outcome Study), cohort, which includes patients with limited cutaneous (lc)  
144 (lcSSc) and diffuse cutaneous (dcSSc) at different stages of disease, and the Prospective  
145 Registry for Early Systemic Sclerosis (PRESS) cohort, enriched for patients with early-  
146 stage dc-SSc. *SIX1* transcript levels were elevated in SSc skin in limited SSc, diffuse  
147 SSc, and in early diffuse SSc compared to control skin in both independent cohorts  
148 (**Figure 1**). In the PRESS cohort, which is enriched for patients with early dcSSc, RNA-  
149 sequencing revealed increased *SIX1* signals (**Figure 1a**). In the GENISOS cohort, which  
150 encompasses dcSSc and lcSSc at different stages of disease, *SIX1* signal intensity,  
151 denoting expression levels, was higher in patients with dcSSc compared to lcSSc (**Figure**  
152 **1b**). To determine whether *SIX1* is associated with the genomic landscape of a particular  
153 cell type, we correlated *SIX1* expression levels with cell type-specific signature scores  
154 previously utilized by our group.(45, 46) The bioinformatic analysis identified genes that  
155 are expressed at comparatively higher levels in a specific cell type and created a  
156 signature score for each cell type being evaluated. The subcutaneous adipose signature  
157 was the most highly correlated with *SIX1* expression in both the GENISOS ( $r = 0.76$ ) and  
158 PRESS cohorts ( $r = 0.79$ ). This points to *SIX1* is an important mediator that is elevated in

159 adipose tissue in SSc (**Figure 1c**). Higher expression of genes specific to fibroblasts,  
160 vascular and lymphatic endothelial cells, significantly correlated with higher expression of  
161 *SIX1*, suggesting that *SIX1* may regulate mesodermal derived cells during fibrosis but not  
162 the ectodermally derived epithelium. Individual gene correlation analysis revealed that  
163 genes associated with adipocyte biology were enriched amongst those genes most highly  
164 correlated with *SIX1*, specifically in early dcSSc skin (**Figure 1d; Supplementary Table**  
165 **3**). These included genes encoding proteins required for adipocyte differentiation and  
166 triglyceride metabolism, including *ADIPOQ* and *PPARG*.(47-49) Functional annotation of  
167 all differentially expressed genes (DEGs) in the skin of dcSSc patients in the PRESS  
168 cohort compared to healthy controls showed significant enrichment for “regulation of  
169 lipolysis in adipocytes” in addition to “ribosome” and “AMPK signaling pathway” (**Figure**  
170 **1e**).

171

### 172 **Increased adipocyte *SIX1* levels correlate with loss of dermal white adipose tissue** 173 **(DWAT) in SSc**

174

175 Several studies have shown that the lipoatrophy and loss of DWAT is present in skin  
176 fibrosis in SSc(15) and even precedes the fibrotic matrix deposition(50). In addition, AMT  
177 (22, 24) and the adipose secretome (26) have been implicated in the pathophysiology of  
178 SSc. Thus, we next aimed to determine whether *SIX1* levels were increased in the  
179 diminishing DWAT layer in the skin. Herein, we assessed tissue samples from the  
180 GENISOS cohort that include SSc-affected skin samples with varying disease durations  
181 were compared to an age, sex, and ethnicity-matched control sample which  
182 demonstrating a progressive loss of DWAT areas as disease progresses (**Figure 2a**).

183 This is important as DWAT levels are known to reduce as dermal fibrosis develops, thus  
184 the GENISOS cohort allows us to temporally assess loss of adipose tissue and *SIX1*  
185 levels during progression of disease. Demographic and clinical features of these  
186 individuals are listed in **Supplementary Table 4**. Compared to the control biopsy, there  
187 was notably less DWAT in the skin of all dcSSc-affected individuals, with the patient with  
188 the most established form of disease presenting with no discernible DWAT areas (**Figure**  
189 **2a**). Thus, having established a correlation between changes in adipocyte biology,  
190 stromal cells, and *SIX1* gene expression in SSc skin; we sought out to identify those cell  
191 types that produce *SIX1* in SSc skin with abnormal dermal fat.

192

193 We selected 8 SSc patients who retained dermal fat, most of whom were within three  
194 years of developing diffuse disease. Additionally, skin biopsies from 4 healthy controls  
195 were included. To localize the *SIX1* gene in these samples, we employed single-molecule  
196 in situ hybridization. DWAT in human skin is localized around adnexal glands and hair  
197 follicles, and within and below the deep dermis(51). *SIX1* was detected in both peri-  
198 adnexal and deep dermal adipocytes. Mature adipocytes are identifiable by a single large  
199 lipid droplet surrounded by a thin ring of cytoplasm and a peripheral nucleus, which  
200 expresses Fatty Acid Binding Protein 4 (*FABP4*) (**Figure 2b**). Our morphometric  
201 quantification revealed increased expression of *SIX1* in SSc tissue (**Figure 2c**). We  
202 acknowledge that some fibroblasts also express *FABP4*, however, the unique  
203 morphology of adipocytes as described above makes them easily distinguishable from  
204 the small, spindle-shaped fibroblast with a dominant, central nucleus. Although *FABP4*<sup>+</sup>  
205 cells are consistent with preadipocytes, it is plausible for subset of cells to include

206 macrophage- or vascular-associated populations. In addition based on landmark scRNA-  
207 seq studies in SSc skin(52), increased SIX1 expression levels in fibroblast and pericyte  
208 subtypes, with limited expression in keratinocytes, macrophages and reduced expression  
209 in endothelial cells (**Supplementary Table 5**). It is important to note that no datasets were  
210 present for mature adipocytes. The clinical relevance of these findings was supported by  
211 positive correlations between the expression of *SIX1* in SSc skin, and the extent and  
212 severity of SSc skin fibrosis. Spearman's rank-order correlation analysis showed a  
213 positive correlation between whole skin *SIX1* expression and modified Rodnan skin score  
214 (mRSS) ( $r=0.40$ ,  $p<0.001$ ), and local skin score ( $r=0.38$ ,  $p<0.001$ ) near the site of the  
215 biopsy. To our knowledge, dermal fat *SIX1* has not previously been identified *in situ*, the  
216 significance of which is supported by clinical data linking *SIX1* to more severe and  
217 extensive SSc skin involvement. Together, these data from two SSc study cohorts  
218 provided a strong premise for investigating *SIX1* in SSc disease mechanisms.

219

## 220 **Adipose tissue loss is evident in a bleomycin model of dermal fibrosis**

221  
222 We selected the murine subcutaneous (SQ) bleo model of skin fibrosis(53) as the pre-  
223 clinical model to study the effects of *SIX1* on fibrosis and lipoatrophy.(11, 54) Unlike  
224 human skin, rodent skin DWAT is separated from the SWAT by a thin layer of skeletal  
225 muscle (the panniculus carnosus), allowing us to distinguish dermal adipocytes from  
226 subcutaneous adipocytes without the use of additional markers.(55, 56) Further, the  
227 fibrotic changes that occur over the 28 days of SQ bleo treatment allow us to study the  
228 role and expression of *SIX1* during the pathogenesis of dermal fibrosis.(22, 50, 57)

229 We demonstrated that serial injections of SQ bleo recapitulated lipodystrophy and dermal  
230 sclerosis mirroring SSc manifestations (**Figure 3a**).<sup>(22, 49, 56)</sup> Using Masson's trichrome  
231 staining, we showed progressive bleo-induced atrophy of the DWAT, increased collagen  
232 deposition, and dermal thickening observable at weekly time points up to 28 days (**Figure**  
233 **3b**). Attrition of DWAT was appreciable on histology as early as day 7 of bleo treatment,  
234 when dermal thickening was less pronounced. Quantification of dermal thickness and  
235 DWAT area confirmed these observations. When compared to day 7, dermal thickening  
236 was significant after 28 days of bleo (**Figure 3c**). This change lagged behind the  
237 significant decline in DWAT area (**Figure 3d**). Transcriptomic analysis revealed increased  
238 signals for *Six1* (**Figure 3e**) and despite minimal histological changes in the dermis after  
239 7 days of bleo, prominent extracellular matrix genes collagen 1a1 (*Col1a1*), collagen 1a2  
240 (*Col1a2*), and collagen 6a1 (*Col6a1*), transforming growth factor beta (*Tgfb1*) and of  
241 serine proteinase inhibitor E 1 (*Serpine1*) were upregulated (**Figure 3f-j**). Intriguingly, we  
242 did not detect increased expression for peroxisome proliferator-activated receptor gamma  
243 (*Pparg*) on day 7 of SQ bleo (**Figure 3k**). These results support that a reduction in DWAT  
244 and upregulation of fibrotic genes precedes significant dermal expansion following SQ  
245 bleo treatment. Next, we investigated whether adipocyte *Six1* expression, as observed in  
246 SSc skin, was recapitulated in the SQ bleo model. Dual in situ hybridization probed for  
247 skin *Six1* and *Adipoq* transcript expression after 7 days of SQ vehicle or bleo injections.  
248 *Adipoq* is highly and specifically expressed in lipid-laden adipocytes.<sup>(48)</sup> Mirroring  
249 findings in human SSc skin whereby *SIX1* was elevated in early disease, *Six1* transcripts  
250 levels were upregulated in the dermal adipocytes after 7 days of SQ bleo treatment  
251 (**Figure 4 a -c**). We also assessed *Six1* expression levels in fibroblasts using smooth

252 muscle actin (SMA) as a readout, these studies did not reveal increased *Six1* in SMA+  
253 cells. (**Figure 4 d, e**). Collectively, this data demonstrates that adipocyte loss is evident  
254 prior to fibrotic deposition and that SIX1 levels are increased in adipocytes by day 7 of  
255 bleo treatment.

256

### 257 **Transgenic *Six1* deletion attenuates bleomycin-induced skin fibrosis**

258

259 We next investigated whether genetic inhibition of *Six1* could prevent skin fibrosis. After  
260 a 28-day course of SQ bleo to induce an end-stage fibrosis phenotype, the affected skin  
261 of tamoxifen-treated mice with (iUbc<sup>Cre</sup>) and without the *Six1* allele (iUbc-*Six1*<sup>-/-</sup>) was  
262 analyzed by gene expression profiling and histology (**Figure 5 a**). *Six1* depletion in iUbc-  
263 *Six1*<sup>-/-</sup> skin following tamoxifen was confirmed morphometrically using dual FABP4 IHC  
264 and Rnascope for *Six1* (**Figure 5 b, c**) and by RT-qPCR (**Figure 5 d**). Expression of  
265 profibrotic agents *Col1a1*, *Col1a2*, *, *elastin*, *Acta2*, *Tgfb1* and *Serpine1* but not *Mif*  
266 was decreased in the skin of iUbc-*Six1*<sup>-/-</sup> compared to iUbc<sup>Cre</sup> mice (**Figure 5 e-l**). To  
267 investigate whether *Six1* modulates latent TGF-β complex components, we measured  
268 Latent Transforming Growth Factor Beta Binding Protein (*Ltbp*)1–4 transcripts. Only  
269 *Ltbp4* but not *Ltbp1-3* was significantly decreased in iUbc-*Six1*<sup>-/-</sup> mice, (**Figure 5, m-p**).  
270 These data suggest that *Six1* may selectively affect latent TGF-β  
271 sequestration/availability through *Ltbp4*. We did not detect changes in expression of  
272 adipocyte markers: *Adiponectin*, *Cebpa*, or *Pparg* (**Figure 5 q-s**). Masson's trichrome  
273 staining of bleo-affected skin showed maintenance of the DWAT layer in iUbc-*Six1*<sup>-/-</sup> mice  
274 compared to iUbc<sup>Cre</sup> mice (**Figure 6a**). *Six1*-deficient mice had more prominent DWAT  
275 with lipid-laden adipocytes (**Figure 6b**). Perilipin 1 immunostaining was used to*

276 specifically detect adipocyte lipid droplets (**Figure 6c**). Adipocyte droplets in iUbc-Six1<sup>-/-</sup>  
277 were significantly larger compared to iUbc<sup>Cre</sup> mice (**Figure 6d**). The deposition of collagen  
278 6, which is enriched in adipose tissue, was analyzed using dual immunofluorescent  
279 staining with perilipin 1 to identify the DWAT (**Figure 6c**). (58, 59) iUbc-Six1<sup>-/-</sup> had lower  
280 collagen 6 density in the DWAT compared to iUbc<sup>Cre</sup> mice (**Figure 6e**). There was no  
281 significant difference in collagen 6 deposition in the dermis, or in dermal thickening (data  
282 not shown). In summary, whole-body depletion of *Six1* followed by 28 days of SQ bleo  
283 revealed that *Six1* deletion may halt pro-fibrotic gene expression and maintain DWAT in  
284 skin fibrosis.

285  
286 **To determine whether adipocyte-derived SIX1 contributes to dermal fibrosis, we**  
287 **examined the effect of adipocyte-specific deletion of Six1 in the bleomycin-induced**  
288 **skin injury model**

289  
290 To build on our data demonstrating elevated *SIX1* in biopsies from individuals with early  
291 SSc and adipose *Six1* expression in a mouse model of dermal fibrosis, when DWAT has  
292 begun to atrophy. We next investigate the potential role of adipocyte-specific *Six1* in early  
293 disease. We developed a transgenic mouse model to knock-out *Six1* in cells with an  
294 active *Adipoq* promoter after tamoxifen treatment, conferring adipocyte-specific *Six1*  
295 depletion in adult mice (48). We challenged mice with SQ vehicle or bleo for 14 days, as  
296 we found this duration of bleo induced DWAT atrophy before late fibrosis is established.  
297 Gene expression and histological analyses were performed to determine the contribution  
298 of adipocyte *Six1* in early events in skin fibrosis. Masson's trichrome staining and dermal  
299 thickness measurements revealed a thinner dermis in iAdipo-Six1<sup>-/-</sup> mice after SQ bleo  
300 compared to iAdipo<sup>Cre</sup> mice (**Figure 7a-b**), demonstrating how adipocyte-specific *Six1*  
301 deletion prevented dermal thickening compared to *Six1*-competent mice. *Six1* deletion

302 was assessed morphometrically in dual RNAscope for *Six1* and adiponectin revealed  
303 reduced *Six1* puncta in Bleo-treated iAdipo-*Six1*<sup>-/-</sup> mice. Gene expression analysis  
304 revealed reduced *Serpine1* but elevated *Adiponectin* expression on day 14 of bleo  
305 exposure in in iAdipo-*Six1*<sup>-/-</sup> vs control iAdipo<sup>Cre</sup> mice (**Figure 7e, f**). Consistent with  
306 improved dermal thickness at day 14 of Bleo, we report reduced *Col1a1* and *Col1a2*  
307 following SQ bleo in iAdipo-*Six1*<sup>-/-</sup> vs control iAdipo<sup>Cre</sup> mice (**Figure 7 g, h**).

308 Next, we performed perilipin 1 immunostaining to identify adipocytes in the DWAT and  
309 measured intracellular lipid droplet size (**Figure 8a**). No difference in droplet size was  
310 observed in vehicle-treated mice regardless of *Six1* expression. However, adipocyte *Six1*  
311 deletion inhibited the reduction in droplet size induced by bleo that precedes loss of  
312 adipose tissue (**Figure 8b**). These findings suggest that *Six1* plays a role in dermal lipid  
313 droplet size during the early development of skin fibrosis. To determine whether adipocyte  
314 preservation was accompanied by reduced DWAT collagen deposition, we performed  
315 immunofluorescent staining to detect collagen 6. While collagens 1, 4, and 6 are  
316 abundantly expressed in adipocytes, collagen 6 is the most predominant collagen in fat  
317 depots (59), thus the measurement of such would be expected to have the highest  
318 sensitivity for significant changes in the ECM. Deletion of *Six1* in adipocytes significantly  
319 reduced DWAT collagen 6 deposition after 14 days of bleo (**Figure 9 a, b**). This is evident  
320 in dual IF for perilipin and collagen 6 demonstrating maintenance of perilipin structures  
321 and reduced COL6 in SQ Bleo treated iAdiponectinCre-*Six1*<sup>-/-</sup> vs iAdiponectin<sup>Cre</sup> controls  
322 (**Figure 9c**). Adipocyte lipid droplet shrinkage and increased ECM deposition cause  
323 dramatic changes to DWAT architecture and function in skin fibrosis. We have here

324 established adipocyte *Six1* as a driver of both lipid droplet size and ECM deposition, and  
325 a candidate target for therapeutic intervention.

326

327 Collectively, our data demonstrates that *Six1* deletion helps maintain lipid droplet size  
328 and ECM deposition in bleomycin-treated mice. To identify the SIX1 downstream  
329 mechanisms, we treated 3T3L1 fibroblasts with a *siSIX1* (or control siRNA) and an  
330 adipocyte differentiation cocktail to promote differentiation to adipose cells. Cells were  
331 collected on days 0, 2, 4, 6 and 9. These experiments demonstrated a reduction *SIX1*  
332 knockdown on day 4 and 6 by western blots (**Supplementary Figure 1 a, b**).

333 Next, we performed a gene analysis using the nCounter platform targeting fibrotic gene  
334 expression on Day 6 of 3T3 treated fibroblasts with and without *siSIX1*. These unbiased  
335 experiments and subsequent heat maps for ECM synthesis and TGF- $\beta$  signaling revealed  
336 that KD of *SIX1* reduced levels of serine proteinase inhibitor E 1 (SERPINE1) the gene  
337 that encodes plasminogen activator inhibitor 1 (PAI-1), (**Supplementary Figure 2 a, b**).

338 These results also demonstrated reduced *Col4a1*, *Col4a2*, *Col5a1* and *Col5a3* and  
339 *Col6a3* in addition to *Tgfb1*. Analysis of the TGF- $\beta$  signaling pathway revealed reduced  
340 downstream mediators following *siSix1* such as *Tgfbr1*, *Crebbp*, or *Furin*  
341 (**Supplementary Figure 2 a, b**). *Serpine1* was selected for further validation based on  
342 a volcano plot demonstrating that it was one of the most significantly downregulated  
343 genes following *siSix1*. (**Supplementary Figure 3**).

344

345 To further investigate the role of *Six1* as a regulator of *Serpine1*, we treated mouse 3T3L1  
346 fibroblasts with a pLenti-CRISPR/Cas9 *Six1* gRNA vector and an adipocyte differentiation

347 cocktail to promote differentiation to adipose cells. Clone 2 was selected for its efficacy  
348 at depleting SIX1 levels, consistent with reduced PAI-1 levels (**Figure 10 a**). Cells were  
349 collected on days (D) 0, 2, 4, 6, 9 and 12, herein *Six1* deletion resulted in reduced  
350 Serpine1 levels on D, 2, 4, 6 and 9 (**Figure 10 b**). The reduction in *Serpine1* expression  
351 levels was consistent with reduced PAI-1 signals in DWAT areas in Bleo-treated  
352 iAdiponectinCre*Six1*<sup>-/-</sup> mice vs control Adiponectin<sup>Cre</sup> mice, assessed morphometrically  
353 (**Figure 10 c, d**). We confirmed *SERPINE1* promoter binding by SIX1 using a full-  
354 length h*SERPINE1* promoter Gaussia Luciferase–expressing plasmid. Luciferase activity  
355 was significantly increased in *Six1*OE within 12 hours indicating a direct activation of the  
356 promoter (**Figure 10 e**). Expression of *SERPINE1* was also upregulated 11.5-fold and  
357 3.8-fold in the PRESS and GENISOS cohorts respectively (**Table 1**). Although the  
358 increased expression of *SERPINE1* could reflect secondary processes in fibrosis, our  
359 findings support the conclusion that SIX1 upregulation directly promotes *SERPINE1*/*PAI*-  
360 1 expression as a downstream driver of dermal fibrosis.

361 Next, to identify whether SIX1 can directly regulate stromal cell fate in dermal fibrosis we  
362 assessed lipid expression levels in mouse 3T3L1 fibroblasts exposed to adipocyte  
363 differentiation cocktail. These studies revealed increased *adiponectin* and *Cebpa*  
364 expression levels on D6, D9 (*Cebpa* only) and D12 of CRISPRCas9 deletion of *Six1*  
365 (**Supplementary Figure 4 a, b**). *Fabp4* and *Pparg* followed the same trend with reduced  
366 expression in SIX1 KD cells of both of these genes on D2 and D9 (*Pparg* only) and  
367 increased expression on D4, D6 and D12 (**Supplementary Figure 4 c, d**). Fibro-genic  
368 gene expression revealed increased *Fn1* expression levels on D0 and D2 but reduced  
369 expression on D6 and D9 (**Supplementary Figure 4 e**) in SIX1 KD cell. *Mif* expression

370 levels reduced on D4, D6 but increased on D12 (**Supplementary Figure 4 f**) following  
371 loss of SIX1. *Tgfb1* expression levels were reduced on D2, D9 and D12 but elevated on  
372 D6, in SIX1 deficient cells (**Supplementary Figure 4 g**). Intriguingly, the downstream  
373 mediator of TGF $\beta$ , *Smad3*, did not follow the same trend as *Tgfb* except for D12 where it  
374 was also reduced; instead, it was reduced on D0, and elevated on D2 and D9  
375 (**Supplementary Figure 4 h**). Despite the variation in gene expression, these data point  
376 to deletion of SIX1 resulting in increased lipid mediators and reduced pro-fibrotic gene  
377 expression by D12. This temporal pattern parallels the *in vivo* sequence, where adipocyte  
378 depletion precedes collagen deposition, suggesting that SIX1 orchestrates early  
379 transcriptional events determining stromal fate after injury. This is consistent with IF  
380 denoting a more adipocyte-like cell following SIX1 KD compared to control cells  
381 stimulated with a differentiation cocktail (**Supplementary Figure 4 i**). These *in vitro*  
382 studies suggest that SIX1 acts to repress adipocyte differentiation and favor a more  
383 fibroblast-like, profibrotic transcriptional state when treated with a adipocyte differentiation  
384 cocktail *in vitro*.

385

## 386 **Discussion**

387 This study demonstrates the previously undescribed clinical and translational relevance  
388 of the developmental transcription factor *SIX1* in adipocyte-mediated skin fibrosis. We  
389 identified increased expression of the developmental transcription factor *SIX1* in skin-  
390 associated adipose tissue in SSc skin samples from two well-described cohorts  
391 encompassing 161 patients. The GENISOS cohort contains both lcSSc and dcSSc,  
392 allowing us to identify a further increase in *SIX1* in diffuse disease in a large cohort. *SIX1*  
393 was also elevated in the skin of individuals with dcSSc diagnosed within three years of  
394 disease onset, obtained from the PRESS cohort. In agreement with expression data  
395 showing enrichment of *SIX1* in dcSSc, *SIX1* skin expression positively correlated with  
396 clinical measurements consistent with worse skin disease extent and severity. Previous  
397 work established a subcutaneous adipose signature in human skin.(45, 46, 60) We found  
398 this signature to be strongly correlated with *SIX1* expression in both SSc cohorts. It is  
399 important to note that a specific dermal adipose signature has not yet been  
400 established.(56) This observation suggests that in SSc skin, *SIX1* expression may be  
401 associated with genomic changes in adipocyte function. Expression data was supported  
402 by histology findings in SSc skin samples from the GENISOS cohort. We reproduced  
403 previously reported observations(15, 50) that dermal fat mass declines early and remains  
404 atrophic in SSc skin. Using two novel transgenic mouse models, we found evidence for a  
405 role for *Six1* in lipodystrophy and fibrotic features observed in the SQ bleo model.  
406 Intriguingly, however, only the deletion of *Six1* from adipocytes but not in UBC<sup>Cre</sup>  
407 expressing mice resulted in a reduction of dermal thickening. Possible explanations for  
408 this include a more efficient and selective inhibition of *Six1* in adipocytes through the

409 adiponectin Cre system compared to UBC<sup>Cre</sup> expression or a potential protective  
410 response of *Six1* in other cells that could include mesenchymal or inflammatory cells. We  
411 propose a working model in which SIX1 helps to drive skin fibrosis by interacting with  
412 lipolysis-associated molecular pathways to promote intracellular lipid loss, a critical first  
413 step towards transforming a healthy adipocyte to a disease-driving cell type. However, it  
414 is also possible for the adipocyte layer to function as a protective element against the  
415 development of fibrosis that is lost as tissue atrophies.

416  
417 We found that *SIX1* expression in SSc skin correlated with genes related to lipid  
418 metabolism. We and others have shown that lipid droplets in DWAT are smaller in the SQ  
419 bleo-treated mice.(22, 61) Mice with *Six1*-deficient adipocytes (*Six1*<sup>-</sup> WAs) had larger  
420 intracellular lipid droplets than *Six1*<sup>+</sup> WAs after SQ bleo. Changes in size of unilocular  
421 lipid droplets in WAs is one surrogate measurement used to profile an adipose depot as  
422 being lipogenic or lipotrophic.(51, 62) A critical step in AMT is the release of free fatty  
423 acids into the local tissue environment, a process which permits the transition of a lipid  
424 droplet-containing adipocyte into a precursor cell(20). AMT is a fluid process involving  
425 dynamic and complex changes in cellular phenotypes and gene expression(24, 63).  
426 Dynamic control of lipid storage is required for differentiation and transdifferentiation (47,  
427 64, 65). We found *Six1* to be expressed in mouse DWAT after just 7 days of bleo. While  
428 the majority of *Six1*-positive (*Six1*<sup>+</sup>) cells were also positive for *Adipoq* (*Adipoq*<sup>+</sup>), we  
429 observed a minority of *Six1*<sup>+</sup> *Adipoq* cells, that is, cells other than lipid-laden adipocytes.  
430 *Adipoq* cells in the stroma vascular fraction (SVF) include diverse cell types.(66) Further,  
431 *ADIPOQ* was highly correlated with *SIX1* in SSc skin. Given the exclusivity of *Six1*  
432 expression to the DWAT, we propose that these cells most likely represent those of

433 adipocyte lineage. These studies and the known capacity of SIX1 to promote trans-  
434 differentiation (38, 67) point at a role for SIX1 in mediating AMT. In line with this, our *in*  
435 *vitro* findings provide mechanistic insight into our *in vivo* observations showing that SIX1  
436 deletion maintains DWAT and adipocyte barrier following fibrotic injury. In cultured 3T3-  
437 L1 fibroblasts, loss of SIX1 enhanced adipogenic differentiation, as evidenced by  
438 increased expression of *Adiponectin*, *Cebpa*, *Pparg*, and *Fabp4*, and reduced expression  
439 of profibrotic mediators including *Fn1*, *Mif*, *Tgfb1*, and *Smad3*. This pattern mirrors the  
440 phenotype observed in SIX1-deficient mice, where adipocytes were preserved and fibrotic  
441 remodeling was attenuated after bleomycin treatment. Together, these data support a  
442 model in which SIX1 promotes AMT by repressing adipogenic transcriptional programs  
443 and activating fibrogenic signaling. Deletion of SIX1 prevents this reprogramming, thereby  
444 stabilizing adipocyte identity and preserving the DWAT barrier. Given the observed  
445 modulation of *Mif* and PAI-1 expressions, SIX1 may also regulate paracrine signaling  
446 between adipocytes and fibroblasts, reinforcing profibrotic activation within the dermal  
447 microenvironment. To further uncover the mechanism that leads to SIX1-mediated  
448 paracrine dermal fibrosis, we turned to a non-biased approach using the nCounter  
449 platform. Here siRNA deletion of *Six1* in 3T3L1 cells inhibited ECM components such as  
450 *Col6a3*, consistent with our IHC for COL6A and other collagens such as *Col4a1*, *Col4a2*,  
451 *Col5a1* and *Col5a3* in addition to *Tgfb1*. In line with previous studies linking *Mif*(30) ,  
452 *Tgfb1*(67) and *Pparg*(43) as targets of SIX1 our studies demonstrated that these  
453 mediators we altered following SIX1 deletion using CRISPRCas9. To further explore  
454 upstream pathways that may link SIX1 to fibrotic remodeling, we examined expression of  
455 *Ltbp* family, which regulates extracellular sequestration and activation of latent TGF- $\beta$

456 complexes(68). Among these, only *Ltbp4* was significantly reduced in Bleo-iUbc-Six1<sup>-/-</sup>  
457 mice. Because LTBP4 participates in matrix tethering and bioavailability of latent TGF-β,  
458 its selective downregulation may attenuate TGF-β activation in the fibrotic niche. These  
459 findings raise the possibility that SIX1 modulates dermal fibrosis in part through regulation  
460 of latent TGF-β signaling. Since LTBP4 regulates extracellular sequestration and  
461 activation of latent TGF-β complexes(69), its reduction in SIX1-deficient mice may  
462 contribute to attenuated TGF-β activation and diminished fibrotic remodeling

463 A common mediator that was altered in both heat maps was *Serpine1*, the gene encoding  
464 for PAI-1. These results revealed reduced *Serpine1* following *Six1* deletion by  
465 CRISPRCas9, a result that was validated by RT-qPCR and western blots and by IHC in  
466 skin sections from bleo-treated mice, revealing reduced PAI-1 signals in mice lacking *Six1*  
467 in adipocytes. This was further confirmed with a luciferase assay demonstrating that SIX1  
468 is able to bind to the *Serpine1* promotor. These results are significant since elevated PAI-  
469 1 has been shown to be elevated in skin lesions from SSc patients(70, 71) and its  
470 inhibition improved dermal inflammation and fibrosis in bleo treated mice.(71) These  
471 findings suggest SIX1 as upstream from PAI-1 and as a mediator that predisposes  
472 adipocytes to a pro-fibrotic phenotype.

473 Although SIX1 expression was most prominent in dermal fibroblasts, increased SIX1  
474 expression was also observed in macrophage-like and endothelial-like cells in both the  
475 GENISOS and PRESS cohorts. The functional significance of SIX1 in these non-fibroblast  
476 populations remains to be determined. It is conceivable that SIX1 contributes to profibrotic  
477 signaling through modulation of cytokine or angiogenic pathways, consistent with its  
478 described roles in other systems (72, 73). Although SIX1 expression was strongest in

479 fibroblast and perivascular clusters, its induction across stromal compartments suggests  
480 a broader contribution to the activated dermal niche in SSc.

481 Targeted therapeutics in SSc are limited as a result of our fragmented understanding of  
482 disease mechanisms.(74) Two medications, nintedanib and tocilizumab, have been  
483 approved by the Food and Drug Administration (FDA) for SSc-related interstitial lung  
484 disease.(75) However, neither these drugs or others are FDA-approved for SSc skin  
485 involvement. SIX1 has been shown to be a potential therapeutic target in pulmonary  
486 fibrosis.(30) We proposed that SIX1 might also play a role in skin fibrosis. We have shown  
487 that genetic deletion of *Six1* is able to reduce dermal adipose tissue atrophy and fibrotic  
488 changes in a rodent model of skin fibrosis. These studies demonstrate that adipose tissue  
489 homeostasis not only has anti-fibrotic effects, but that its preservation is a potential  
490 therapeutic approach for skin manifestations in SSc. Although our data support a primary  
491 role for SIX1 in adipocyte fate determination, its regulation of inflammatory mediators  
492 such as MIF suggests that SIX1 may also influence immune-stromal interactions  
493 contributing to sustained fibrosis. Together, these findings suggest that pharmacological  
494 inhibition of SIX1, or its downstream mediator PAI-1, may represent a novel strategy for  
495 preventing or treating dermal fibrosis in SSc.

496

497 **Methods**

498 **Sex as a biological variant**

499 In our human and mouse studies female and male sexes were examined no significant  
500 differences were observed between sexes.

501

502 **Study populations**

503 *GENISOS cohort*

504

505 The prospective cohort study, GENISOS , is a collaboration between The University of  
506 Texas Health Science Center, Houston, The University of Texas Medical Branch at  
507 Galveston, and the University of Texas Health Science Center at San Antonio. All  
508 participants met the diagnosis of SSc according to the American College of  
509 Rheumatology preliminary classification.(76) Details of recruitment and selection criteria  
510 have been previously published.(77) As described by (78), full-thickness skin biopsies  
511 (forearm or back) were collected under local anesthesia. Total RNA was extracted using  
512 TRizol reagent (Invitrogen) followed by RNeasy column purification (Qiagen). RNA  
513 integrity was confirmed (RIN > 7) before hybridization to the Illumina HumanHT-12 v4  
514 Expression BeadChip.

515 Individuals with dcSSc and lcSSc are enrolled within five years of disease onset, defined  
516 as the first non-Raynaud's symptom. The study was approved by the institutional review  
517 board of all participating sites, and written informed consent was obtained from all study  
518 subjects.

519 The mRSS was calculated by a board-certified rheumatologist with extensive experience  
520 in the assessment of scleroderma skin (79). The mRSS is determined by assessment of  
521 the skin thickness of 17 body areas by physical examination. The mRSS serves as a  
522 surrogate for disease activity, severity and mortality in patients with SSc (80). Healthy

523 control individuals are enrolled to serve as controls. SSc-affected individuals and controls  
524 are matched at a ratio of 3:1 based on age, sex, and ethnicity. Gene expression analysis  
525 from SSc-affected skin and skin from controls has been previously described.(78) Raw  
526 probe-level intensities were imported into BRB-ArrayTools v4.7.1, log<sub>2</sub>-transformed, and  
527 quantile-normalized. Probes with > 20 % missing values or mean signal below  
528 background were excluded prior to differential expression analysis. Briefly, global gene  
529 expression is assessed using the Illumina HumanHT-12 bead array. Raw data were  
530 analyzed with BRB ArrayTools. 113 SSc-affected individuals and 44 unaffected controls  
531 had available *SIX1* expression levels.

532

### 533 *PRESS cohort*

534

535 The PRESS cohort is a multi-site observational cohort of individuals with dcSSc enrolled  
536 within three years of the onset of the first non-Raynaud's symptom.(9) All participants  
537 fulfill the 2013 American College of Rheumatology (ACR)/European League Against  
538 Rheumatism (EULAR) classification criteria for SSc.(81) RNA sequencing data from the  
539 skin of PRESS participants and controls, previously utilized by our group,(46) was queried  
540 for expression of *SIX1*. Forty-eight SSc-affected individuals and thirty-three controls had  
541 available *SIX1* expression levels. RNA-seq libraries were generated from total RNA using  
542 the Illumina TruSeq Stranded mRNA kit and sequenced (2 × 100 bp) on a HiSeq 2500.  
543 Reads were aligned to the human GRCh38 reference genome using STAR v2.7, and raw  
544 counts were normalized and tested for differential expression with edgeR (82). The R  
545 Bioconductor package edgeR6 analysis was utilized to identify differentially expressed

546 transcripts between SSc patients and healthy controls with a false discovery rate cutoff  
547 of 0.05 and fold change cutoff of  $>1.5$  or  $<0.67$

### 548 549 **Cell type-specific expression signatures**

550  
551 Cell type-specific expression signatures were originally developed as previously  
552 described (60) and have been utilized by our group.(46) A “cell-type specific signature  
553 score” denotes a set of genes for which expression in a given cell type is notably higher  
554 than expression in the other evaluated cell types. Signature matrices were derived from  
555 previously published SSc skin transcriptomic datasets (83, 84). For each sample, the  
556 mean fold-change (SSc vs control) across 125 signature genes defined the cell-type  
557 score. Spearman’s rank correlations were computed between each score and SIX1  
558 expression to assess lineage association. The numerical value of each score was  
559 calculated based on fold-change estimates (SSc versus control) for 125 “signature genes”  
560 of a given cell type. The methodology used is described in detail in (60, 78, 85), for gene  
561 expression analysis, data were imported into BRB-ArrayTools as processed signal  
562 values. Values were excluded if the mean signal was not significantly greater than the  
563 background. Values were then log<sub>2</sub> transformed, followed by quantile normalization.  
564 Genes with  $>20\%$  missing values across arrays were filtered out. The remaining gene  
565 values were used for analyses.

### 566 567 **Pathway Analysis**

568 Herein, we used the same protocol described previously(60, 78, 85), genes that were  
569 differentially expressed on average in SSc compared to control at a false discovery rate

570 (FDR) of  $<0.05$  were uploaded to Ingenuity Pathway Analysis (Qiagen). The reference  
571 set was 'Human Genome CGH 44 K'; only experimentally observed direct and indirect  
572 relationships were included. Canonical pathway and upstream-regulator analyses were  
573 performed at FDR-adjusted  $P < 0.05$  and confirmed with  $FDR < 0.1$ .

574

### 575 **Correlation analyses**

576

577 The correlation between signature score and *SIX1* expression was evaluated for each  
578 sample, and then the mean Spearman's rank correlation coefficient was reported.  
579 Individual gene correlations were analyzed by Spearman's rank correlation. Correlation  
580 coefficients are reported as "r." All correlation analyses were performed in R v4.2 using  
581 the 'Hmisc' package; significance was defined as two-tailed  $P < 0.05$ . Plots were  
582 generated in ggplot2.

583

### 584 **Functional annotation of all differentially expressed genes in PRESS**

585

586 All DEGs in the skin biopsies of PRESS cohort participants with SSc were input into The  
587 **Database for Annotation, Visualization and Integrated Discovery (DAVID)** for functional  
588 annotation (Available at <https://david.ncifcrf.gov/summary.jsp>). Analyses were conducted  
589 in DAVID v6.8(86) using the full human genome as background. Biological processes and  
590 molecular functions were considered enriched at Bonferroni-adjusted  $P < 0.05$ . A  
591 Bonferroni cut-off of 0.5 was used to determine significantly enriched biological pathways.

592

593 **Animal studies**

594

595 All studies were reviewed and approved by UTHealth Houston Animal Welfare Committee  
596 (AWC-19-0029, AWC-22-0028). Six to eight-week-old male and female C57/BL6J mice  
597 were used for experiments with wild-type mice. Mice with dorsal skin in the telogen phase  
598 of hair cycle were used. Regions of skin in the anagen phase were excluded. When  
599 possible, littermates were equally distributed between groups. Group sizes were  
600 determined by power analysis ( $\alpha = 0.05$ , power = 80%) and restricted to telogen-phase  
601 skin, as exclusion of anagen-phase regions reduces biological variability and provides  
602 reliable statistical power with fewer animals(87).

603 Detailed experimental procedures are available in the supplement, including a complete  
604 list of SYBR green primers is listed in Supplementary Table 1.

605

606 **Statistical analysis**

607

608 Prism software (v9.0; GraphPad or higher) was used for all statistical analyses. ROUT  
609 outlier test was performed on all datasets. Outliers were excluded if FDR was greater  
610 than 1%. Two-tailed t-test with Welch's correction was used for 2-group comparisons.  
611 Two-way ANOVA with multiple comparisons and correction using the Sidak method was  
612 used for 3 or more groups. Detailed statistical analysis for each experiment is shown in  
613 the figure legends.

614 **Declarations:**

615 **Author Contributions:** NW, SA, and HKQ conducted experiments, acquired data,  
616 analyzed data, and wrote the manuscript. TM, SC, MW, LR, RG, ML, BS, and WB

617 conducted experiments, acquired data, and analyzed data. WS analyzed data and  
618 provided research material. MA, YY and WJZ performed bioinformatic analyses and AF  
619 and HK perform ran the nCounter experiments. All authors read and approved the  
620 manuscript for submission.

621

622 **Funding:** Rheumatology Research Foundation Future Physician Scientist Award  
623 (Wareing); NIH (NHLBI) R01HL138510, R01HL157100 (Karmouty-Quintana); National  
624 Scleroderma Foundation Established Investigator Award (Karmouty-Quintana);  
625 NIH/NIAMS R01AR073284 (Assassi-Mills), NIH/NIAMS R01AR081280 (Assassi-Wu),  
626 NIH/NIAMS K08AR081402 (Skaug), Rheumatology Research Foundation Investigator  
627 Award (Skaug) NIH 1UL1TR003167 (W Jim Zheng) DoD W81XWH-22-1-0164 (W Jim  
628 Zheng).

629

630 **Acknowledgments:** Susan Majka, PhD for critically reviewing the manuscript.

631 **Ethics approval and consent to participate:** We acknowledge PRESS and GENISOS  
632 investigators for their contribution to sample and data collection. Animal experiments  
633 were approved by UTHHealth Houston Animal Welfare Committee as noted in the  
634 methods section. **Availability of data and materials:** The datasets during and/or  
635 analyzed during the current study are available from the corresponding author upon  
636 reasonable request. **Competing Interests:** The authors declare that they have no  
637 competing interests. **Authors information:** NW is currently at Emory University, LR is  
638 currently at Rutgers University, AF is currently at Vanderbilt University.

639

640

641

642

643

644

645

## 646 **References**

- 647 1. Denton CP, and Khanna D. Systemic sclerosis. *Lancet*. 2017;390(10103):1685-  
648 99.

- 649 2. Asano Y. Systemic sclerosis. *J Dermatol*. 2018;45(2):128-38.
- 650 3. Verrecchia F, Laboureau J, Verola O, Roos N, Porcher R, Bruneval P, et al. Skin  
651 involvement in scleroderma--where histological and clinical scores meet.  
652 *Rheumatology (Oxford, England)*. 2007;46(5):833-41.
- 653 4. Ferri C, Valentini G, Cozzi F, Sebastiani M, Michelassi C, La Montagna G, et al.  
654 Systemic sclerosis: demographic, clinical, and serologic features and survival in  
655 1,012 Italian patients. *Medicine*. 2002;81(2):139-53.
- 656 5. Ingegnoli F, Ughi N, and Mihai C. Update on the epidemiology, risk factors, and  
657 disease outcomes of systemic sclerosis. *Best practice & research Clinical*  
658 *rheumatology*. 2018;32(2):223-40.
- 659 6. Postlethwaite AE, Shigemitsu H, and Kanangat S. Cellular origins of fibroblasts:  
660 possible implications for organ fibrosis in systemic sclerosis. *Curr Opin*  
661 *Rheumatol*. 2004;16(6):733-8.
- 662 7. Tyndall AJ, Bannert B, Vonk M, Airò P, Cozzi F, Carreira PE, et al. Causes and  
663 risk factors for death in systemic sclerosis: a study from the EULAR Scleroderma  
664 Trials and Research (EUSTAR) database. *Ann Rheum Dis*. 2010;69(10):1809-  
665 15.
- 666 8. Herrick AL, Assassi S, and Denton CP. Skin involvement in early diffuse  
667 cutaneous systemic sclerosis: an unmet clinical need. *Nat Rev Rheumatol*.  
668 2022;18(5):276-85.
- 669 9. Frech TM, Shanmugam VK, Shah AA, Assassi S, Gordon JK, Hant FN, et al.  
670 Treatment of early diffuse systemic sclerosis skin disease. *Clin Exp Rheumatol*.  
671 2013;31(2 Suppl 76):166-71.
- 672 10. Collum SD, Molina JG, Hanmandlu A, Bi W, Pedroza M, Mertens TCJ, et al.  
673 Adenosine and hyaluronan promote lung fibrosis and pulmonary hypertension in  
674 combined pulmonary fibrosis and emphysema. *Dis Model Mech*. 2019;12(5).
- 675 11. Karmouty-Quintana H, Molina JG, Philip K, Bellocchi C, Gudenkauf B, Wu M, et  
676 al. The Antifibrotic Effect of A(2B) Adenosine Receptor Antagonism in a Mouse  
677 Model of Dermal Fibrosis. *Arthritis Rheumatol*. 2018;70(10):1673-84.
- 678 12. Khanna D, Lin CJ, Furst DE, Goldin J, Kim G, Kuwana M, et al. Tocilizumab in  
679 systemic sclerosis: a randomised, double-blind, placebo-controlled, phase 3 trial.  
680 *The Lancet Respiratory Medicine*. 2020;8(10):963-74.
- 681 13. Pedroza M, To S, Assassi S, Wu M, Tweardy D, and Agarwal SK. Role of STAT3  
682 in skin fibrosis and transforming growth factor beta signalling. *Rheumatology*  
683 *(Oxford, England)*. 2018;57(10):1838-50.
- 684 14. Wirsdörfer F, de Leve S, Cappuccini F, Eldh T, Meyer AV, Gau E, et al.  
685 Extracellular Adenosine Production by ecto-5'-Nucleotidase (CD73) Enhances  
686 Radiation-Induced Lung Fibrosis. *Cancer Res*. 2016;76(10):3045-56.
- 687 15. Varga J, and Marangoni RG. Systemic sclerosis in 2016: Dermal white adipose  
688 tissue implicated in SSc pathogenesis. *Nat Rev Rheumatol*. 2017;13(2):71-2.
- 689 16. Marangoni RG, Varga J, and Tourtellotte WG. Animal models of scleroderma:  
690 recent progress. *Current opinion in rheumatology*. 2016;28(6):561-70.
- 691 17. Zhang Z, Shao M, Hepler C, Zi Z, Zhao S, An YA, et al. Dermal adipose tissue  
692 has high plasticity and undergoes reversible dedifferentiation in mice. *J Clin*  
693 *Invest*. 2019;129(12):5327-42.

- 694 18. Kruglikov IL, and Scherer PE. Skin aging: are adipocytes the next target? *Aging*  
695 (*Albany NY*). 2016;8(7):1457-69.
- 696 19. Majka SM, Barak Y, and Klemm DJ. Concise review: adipocyte origins: weighing  
697 the possibilities. *Stem Cells*. 2011;29(7):1034-40.
- 698 20. Kruglikov IL, Zhang Z, and Scherer PE. Skin aging: Dermal adipocytes  
699 metabolically reprogram dermal fibroblasts. *Bioessays*. 2022;44(1):e2100207.
- 700 21. Shook BA, Wasko RR, Mano O, Rutenberg-Schoenberg M, Rudolph MC, Zirak  
701 B, et al. Dermal Adipocyte Lipolysis and Myofibroblast Conversion Are Required  
702 for Efficient Skin Repair. *Cell Stem Cell*. 2020;26(6):880-95.e6.
- 703 22. Marangoni RG, Korman BD, Wei J, Wood TA, Graham LV, Whitfield ML, et al.  
704 Myofibroblasts in murine cutaneous fibrosis originate from adiponectin-positive  
705 intradermal progenitors. *Arthritis Rheumatol*. 2015;67(4):1062-73.
- 706 23. Onuora S. Connective tissue diseases: Adipocyte-myofibroblast transition: linking  
707 intradermal fat loss to skin fibrosis in SSc. *Nat Rev Rheumatol*. 2015;11(2):63.
- 708 24. Marangoni RG, Korman B, and Varga J. Adipocytic Progenitor Cells Give Rise to  
709 Pathogenic Myofibroblasts: Adipocyte-to-Mesenchymal Transition and Its  
710 Emerging Role in Fibrosis in Multiple Organs. *Curr Rheumatol Rep*.  
711 2020;22(11):79.
- 712 25. Schmidt BA, and Horsley V. Intradermal adipocytes mediate fibroblast  
713 recruitment during skin wound healing. *Development*. 2013;140(7):1517-27.
- 714 26. Brezovec N, Burja B, and Lakota K. Adipose tissue and adipose secretome in  
715 systemic sclerosis. *Current opinion in rheumatology*. 2021;33(6):505-13.
- 716 27. Cooper PO, Haas MR, Noonepalle SKR, and Shook BA. Dermal Drivers of  
717 Injury-Induced Inflammation: Contribution of Adipocytes and Fibroblasts. *Int J*  
718 *Mol Sci*. 2021;22(4).
- 719 28. Zhang Z, Kruglikov I, Zhao S, Zi Z, Gliniak CM, Li N, et al. Dermal adipocytes  
720 contribute to the metabolic regulation of dermal fibroblasts. *Exp Dermatol*.  
721 2021;30(1):102-11.
- 722 29. Crewe C, Joffin N, Rutkowski JM, Kim M, Zhang F, Towler DA, et al. An  
723 Endothelial-to-Adipocyte Extracellular Vesicle Axis Governed by Metabolic State.  
724 *Cell*. 2018;175(3):695-708.e13.
- 725 30. Wilson C, Mertens TC, Shivshankar P, Bi W, Collum SD, Wareing N, et al. *Sine*  
726 *oculis* homeobox homolog 1 plays a critical role in pulmonary fibrosis. *JCI Insight*.  
727 2022;7(10).
- 728 31. Liu S, Chen X, Zhang S, Wang X, Du X, Chen J, et al. miR-106b-5p targeting  
729 SIX1 inhibits TGF- $\beta$ 1-induced pulmonary fibrosis and  
730 epithelial-mesenchymal transition in asthma through regulation of E2F1. *Int J Mol*  
731 *Med*. 2021;47(3).
- 732 32. Yang ZC, Qu ZH, Yi MJ, Shan YC, Ran N, Xu L, et al. MiR-448-5p inhibits TGF-  
733  $\beta$ 1-induced epithelial-mesenchymal transition and pulmonary fibrosis by targeting  
734 Six1 in asthma. *J Cell Physiol*. 2019;234(6):8804-14.
- 735 33. Xu B, Yang Q, Tang Y, Tan Z, Fu H, Peng J, et al. SIX1/EYA1 are novel liver  
736 damage biomarkers in chronic hepatitis B and other liver diseases. *Ann Transl*  
737 *Med*. 2021;9(12):992.

- 738 34. Asano Y. The Pathogenesis of Systemic Sclerosis: An Understanding Based on  
739 a Common Pathologic Cascade across Multiple Organs and Additional Organ-  
740 Specific Pathologies. *J Clin Med.* 2020;9(9).
- 741 35. Kong D, Liu Y, Liu Q, Han N, Zhang C, Pestell RG, et al. The retinal  
742 determination gene network: from developmental regulator to cancer therapeutic  
743 target. *Oncotarget.* 2016;7(31):50755-65.
- 744 36. Kumar JP. The sine oculis homeobox (SIX) family of transcription factors as  
745 regulators of development and disease. *Cell Mol Life Sci.* 2009;66(4):565-83.
- 746 37. Ono H, Imoto I, Kozaki K, Tsuda H, Matsui T, Kurasawa Y, et al. SIX1 promotes  
747 epithelial-mesenchymal transition in colorectal cancer through ZEB1 activation.  
748 *Oncogene.* 2012;31(47):4923-34.
- 749 38. Zhou H, Blevins MA, Hsu JY, Kong D, Galbraith MD, Goodspeed A, et al.  
750 Identification of a Small-Molecule Inhibitor That Disrupts the SIX1/EYA2  
751 Complex, EMT, and Metastasis. *Cancer research.* 2020;80(12):2689-702.
- 752 39. Xu H, Pirisi L, and Creek KE. Six1 overexpression at early stages of HPV16-  
753 mediated transformation of human keratinocytes promotes differentiation  
754 resistance and EMT. *Virology.* 2015;474:144-53.
- 755 40. Smith AL, Iwanaga R, Drasin DJ, Micalizzi DS, Vartuli RL, Tan AC, et al. The  
756 miR-106b-25 cluster targets Smad7, activates TGF- $\beta$  signaling, and induces  
757 EMT and tumor initiating cell characteristics downstream of Six1 in human breast  
758 cancer. *Oncogene.* 2012;31(50):5162-71.
- 759 41. McCoy EL, Iwanaga R, Jedlicka P, Abbey NS, Chodosh LA, Heichman KA, et al.  
760 Six1 expands the mouse mammary epithelial stem/progenitor cell pool and  
761 induces mammary tumors that undergo epithelial-mesenchymal transition. *J Clin*  
762 *Invest.* 2009;119(9):2663-77.
- 763 42. Schleinitz D, Krause K, Wohland T, Gebhardt C, Linder N, Stumvoll M, et al.  
764 Identification of distinct transcriptome signatures of human adipose tissue from  
765 fifteen depots. *European Journal of Human Genetics.* 2020;28(12):1714-25.
- 766 43. Brunmeir R, Wu J, Peng X, Kim SY, Julien SG, Zhang Q, et al. Comparative  
767 Transcriptomic and Epigenomic Analyses Reveal New Regulators of Murine  
768 Brown Adipogenesis. *PLoS Genet.* 2016;12(12):e1006474.
- 769 44. Gao X, Chu Y, Wang W, Li W, Zhang W, Cao J, et al. Detrimental role of SIX1 in  
770 hepatic lipogenesis and fibrosis of non-alcoholic fatty liver disease. *Liver Int.*  
771 2023;43(7):1473-85.
- 772 45. Assassi S, Swindell WR, Wu M, Tan FD, Khanna D, Furst DE, et al. Dissecting  
773 the heterogeneity of skin gene expression patterns in systemic sclerosis. *Arthritis*  
774 *Rheumatol.* 2015;67(11):3016-26.
- 775 46. Skaug B, Khanna D, Swindell WR, Hinchcliff ME, Frech TM, Steen VD, et al.  
776 Global skin gene expression analysis of early diffuse cutaneous systemic  
777 sclerosis shows a prominent innate and adaptive inflammatory profile. *Ann*  
778 *Rheum Dis.* 2020;79(3):379-86.
- 779 47. Grabner GF, Xie H, Schweiger M, and Zechner R. Lipolysis: cellular mechanisms  
780 for lipid mobilization from fat stores. *Nat Metab.* 2021;3(11):1445-65.
- 781 48. Trujillo ME, and Scherer PE. Adiponectin--journey from an adipocyte secretory  
782 protein to biomarker of the metabolic syndrome. *J Intern Med.* 2005;257(2):167-  
783 75.

- 784 49. Ahmadian M, Suh JM, Hah N, Liddle C, Atkins AR, Downes M, et al. PPAR $\gamma$   
785 signaling and metabolism: the good, the bad and the future. *Nat Med*.  
786 2013;19(5):557-66.
- 787 50. Fleischmajer R, Damiano V, and Nedwich A. Alteration of subcutaneous tissue in  
788 systemic scleroderma. *Arch Dermatol*. 1972;105(1):59-66.
- 789 51. Nicu C, Pople J, Bonsell L, Bhogal R, Ansell DM, and Paus R. A guide to  
790 studying human dermal adipocytes in situ. *Exp Dermatol*. 2018;27(6):589-602.
- 791 52. Tabib T, Huang M, Morse N, Papazoglou A, Behera R, Jia M, et al. Myofibroblast  
792 transcriptome indicates SFRP2hi fibroblast progenitors in systemic sclerosis skin.  
793 *Nature Communications*. 2021;12(1):4384.
- 794 53. Yamamoto T, Takagawa S, Katayama I, Yamazaki K, Hamazaki Y, Shinkai H, et  
795 al. Animal model of sclerotic skin. I: Local injections of bleomycin induce sclerotic  
796 skin mimicking scleroderma. *J Invest Dermatol*. 1999;112(4):456-62.
- 797 54. Wu M, Skaug B, Bi X, Mills T, Salazar G, Zhou X, et al. Interferon regulatory  
798 factor 7 (IRF7) represents a link between inflammation and fibrosis in the  
799 pathogenesis of systemic sclerosis. *Ann Rheum Dis*. 2019;78(11):1583-91.
- 800 55. Sbarbati A, Accorsi D, Benati D, Marchetti L, Orsini G, Rigotti G, et al.  
801 Subcutaneous adipose tissue classification. *Eur J Histochem*. 2010;54(4):e48.
- 802 56. Schneider MR. Coming home at last: dermal white adipose tissue. *Exp Dermatol*.  
803 2014;23(9):634-5.
- 804 57. Yamamoto T. Animal model of systemic sclerosis. *J Dermatol*. 2010;37(1):26-41.
- 805 58. Pasarica M, Gowronska-Kozak B, Burk D, Remedios I, Hymel D, Gimble J, et al.  
806 Adipose tissue collagen VI in obesity. *J Clin Endocrinol Metab*.  
807 2009;94(12):5155-62.
- 808 59. Khan T, Muise ES, Iyengar P, Wang ZV, Chandalia M, Abate N, et al. Metabolic  
809 dysregulation and adipose tissue fibrosis: role of collagen VI. *Mol Cell Biol*.  
810 2009;29(6):1575-91.
- 811 60. Swindell WR, Johnston A, Voorhees JJ, Elder JT, and Gudjonsson JE.  
812 Dissecting the psoriasis transcriptome: inflammatory- and cytokine-driven gene  
813 expression in lesions from 163 patients. *BMC genomics*. 2013;14:527.
- 814 61. Jussila AR, Zhang B, Caves E, Kirti S, Steele M, Hamburg-Shields E, et al. Skin  
815 Fibrosis and Recovery Is Dependent on Wnt Activation via DPP4. *J Invest*  
816 *Dermatol*. 2022;142(6):1597-606.e9.
- 817 62. Schweiger M, Eichmann TO, Taschler U, Zimmermann R, Zechner R, and Lass  
818 A. Measurement of lipolysis. *Methods Enzymol*. 2014;538:171-93.
- 819 63. Martins V, Gonzalez De Los Santos F, Wu Z, Capelozzi V, Phan SH, and Liu T.  
820 FIZZ1-induced myofibroblast transdifferentiation from adipocytes and its potential  
821 role in dermal fibrosis and lipotrophy. *Am J Pathol*. 2015;185(10):2768-76.
- 822 64. Stern JH, Rutkowski JM, and Scherer PE. Adiponectin, Leptin, and Fatty Acids in  
823 the Maintenance of Metabolic Homeostasis through Adipose Tissue Crosstalk.  
824 *Cell Metab*. 2016;23(5):770-84.
- 825 65. Ahmad B, Serpell CJ, Fong IL, and Wong EH. Molecular Mechanisms of  
826 Adipogenesis: The Anti-adipogenic Role of AMP-Activated Protein Kinase. *Front*  
827 *Mol Biosci*. 2020;7:76.

- 828 66. Muller S, Ader I, Creff J, Leménager H, Achard P, Casteilla L, et al. Human  
829 adipose stromal-vascular fraction self-organizes to form vascularized adipose  
830 tissue in 3D cultures. *Sci Rep*. 2019;9(1):7250.
- 831 67. Wang W, Yang Z, Li M, Wang Z, Shan Y, and Qu Z. Six1 Promotes Epithelial-  
832 Mesenchymal Transition in Bronchial Epithelial Cells via the TGF $\beta$ 1/Smad  
833 Signalling Pathway. *Int Arch Allergy Immunol*. 2021;182(6):479-88.
- 834 68. Robertson IB, and Rifkin DB. Regulation of the Bioavailability of TGF- $\beta$  and TGF-  
835  $\beta$ -Related Proteins. *Cold Spring Harb Perspect Biol*. 2016;8(6).
- 836 69. Horiguchi M, Ota M, and Rifkin DB. Matrix control of transforming growth factor- $\beta$   
837 function. *J Biochem*. 2012;152(4):321-9.
- 838 70. Postiglione L, Montuori N, Riccio A, Di Spigna G, Salzano S, Rossi G, et al. The  
839 plasminogen activator system in fibroblasts from systemic sclerosis. *Int J*  
840 *Immunopathol Pharmacol*. 2010;23(3):891-900.
- 841 71. Lemaire R, Burwell T, Sun H, Delaney T, Bakken J, Cheng L, et al. Resolution of  
842 Skin Fibrosis by Neutralization of the Antifibrinolytic Function of Plasminogen  
843 Activator Inhibitor 1. *Arthritis Rheumatol*. 2016;68(2):473-83.
- 844 72. Liu W, Gao M, Li L, Chen Y, Fan H, Cai Q, et al. Homeoprotein SIX1  
845 compromises antitumor immunity through TGF- $\beta$ -mediated regulation of  
846 collagens. *Cellular & Molecular Immunology*. 2021;18(12):2660-72.
- 847 73. Zhan H, Chen H, Tang Z, Liu S, Xie K, and Wang H. SIX1 attenuates  
848 inflammation and rheumatoid arthritis by silencing MyD88-dependent TLR1/2  
849 signaling. *International Immunopharmacology*. 2022;106:108613.
- 850 74. Asano Y. Recent advances in the treatment of skin involvement in systemic  
851 sclerosis. *Inflamm Regen*. 2017;37:12.
- 852 75. Khanna D, Lescoat A, Roofeh D, Bernstein EJ, Kazerooni EA, Roth MD, et al.  
853 Systemic Sclerosis-Associated Interstitial Lung Disease: How to Incorporate Two  
854 Food and Drug Administration-Approved Therapies in Clinical Practice. *Arthritis*  
855 *Rheumatol*. 2022;74(1):13-27.
- 856 76. Preliminary criteria for the classification of systemic sclerosis (scleroderma).  
857 Subcommittee for scleroderma criteria of the American Rheumatism Association  
858 Diagnostic and Therapeutic Criteria Committee. *Arthritis Rheum*. 1980;23(5):581-  
859 90.
- 860 77. Reveille JD, Fischbach M, McNearney T, Friedman AW, Aguilar MB, Lisse J, et  
861 al. Systemic sclerosis in 3 US ethnic groups: a comparison of clinical,  
862 sociodemographic, serologic, and immunogenetic determinants. *Semin Arthritis*  
863 *Rheum*. 2001;30(5):332-46.
- 864 78. Skaug B, Lyons MA, Swindell WR, Salazar GA, Wu M, Tran TM, et al. Large-  
865 scale analysis of longitudinal skin gene expression in systemic sclerosis reveals  
866 relationships of immune cell and fibroblast activity with skin thickness and a trend  
867 towards normalisation over time. *Annals of the rheumatic diseases*.  
868 2022;81(4):516-23.
- 869 79. Clements P, Lachenbruch P, Siebold J, White B, Weiner S, Martin R, et al. Inter  
870 and intraobserver variability of total skin thickness score (modified Rodnan TSS)  
871 in systemic sclerosis. *J Rheumatol*. 1995;22(7):1281-5.

- 872 80. Khanna D, Furst DE, Clements PJ, Allanore Y, Baron M, Czirjak L, et al.  
873 Standardization of the modified Rodnan skin score for use in clinical trials of  
874 systemic sclerosis. *Journal of scleroderma and related disorders*. 2017;2(1):11-8.
- 875 81. van den Hoogen F, Khanna D, Fransen J, Johnson SR, Baron M, Tyndall A, et  
876 al. 2013 classification criteria for systemic sclerosis: an American college of  
877 rheumatology/European league against rheumatism collaborative initiative. *Ann*  
878 *Rheum Dis*. 2013;72(11):1747-55.
- 879 82. Robinson MD, McCarthy DJ, and Smyth GK. edgeR: a Bioconductor package for  
880 differential expression analysis of digital gene expression data. *Bioinformatics*.  
881 2010;26(1):139-40.
- 882 83. Milano A, Pendergrass SA, Sargent JL, George LK, McCalmont TH, Connolly  
883 MK, et al. Molecular Subsets in the Gene Expression Signatures of Scleroderma  
884 Skin. *PLOS ONE*. 2008;3(7):e2696.
- 885 84. Whitfield ML, Finlay DR, Murray JI, Troyanskaya OG, Chi JT, Pergamenschikov  
886 A, et al. Systemic and cell type-specific gene expression patterns in scleroderma  
887 skin. *Proc Natl Acad Sci U S A*. 2003;100(21):12319-24.
- 888 85. Swindell WR, Stuart PE, Sarkar MK, Voorhees JJ, Elder JT, Johnston A, et al.  
889 Cellular dissection of psoriasis for transcriptome analyses and the post-GWAS  
890 era. *BMC Med Genomics*. 2014;7:27.
- 891 86. Huang da W, Sherman BT, and Lempicki RA. Bioinformatics enrichment tools:  
892 paths toward the comprehensive functional analysis of large gene lists. *Nucleic*  
893 *Acids Res*. 2009;37(1):1-13.
- 894 87. Wang WH, Ramos R, Tai KY, Wu YS, Chang TY, Yan JY, et al. Studying Hair  
895 Growth Cycle and its Effects on Mouse Skin. *J Invest Dermatol*.  
896 2023;143(9):1638-45.  
897  
898  
899  
900  
901

902 **Figure Legends**

903

904 **Figure 1. *SIX1* is elevated in SSc skin and correlates with adipose-related genes**  
905 **and pathways.**

906 a) *SIX1* expression in PRESS SSc skin samples and controls. FPKM = fragments per  
907 kilobase million based on a false discovery rate cutoff of 0.05 and fold change cutoff of  
908 >1.5 or <0.6 b) *SIX1* expression in baseline SSc skin samples and controls in the  
909 GENISOS cohort based on Student's t-test c) Heatmap showing correlation ("r")  
910 between skin *SIX1* expression and cell type signature scores on Spearman's Rank  
911 order correlation. Bolded pathways indicate correlations with p-values <0.05 in both  
912 cohorts. d) Volcano plot showing individual gene-*SIX1* correlations in PRESS cohort  
913 SSc skin samples. PLIN1=perilipin 1; G0S2=G0/G2 switch gene 2;  
914 ADIPOQ=adiponectin; HSL=hormone sensitive lipase; FABP4=fatty acid binding protein  
915 4; LEP=leptin; ATGL=adipose triglyceride lipase; PPARG= peroxisome proliferator  
916 activated receptor gamma based on a Spearman's rank coefficient analysis. e) KEGG  
917 pathway annotation of all DEGs in SSc skin of PRESS cohort participants using  
918 GoStats. Significance levels \*\*\*  $P \leq 0.001$  refer to a Bonferroni cut-off of 0.5 analysis  
919 (panel a) or a the R Bioconductor package edgeR6 analysis for to identify differentially  
920 expressed transcripts between SSc patients and healthy controls with a false discovery  
921 rate cutoff of 0.05 and fold change cutoff of >1.5 or <0.67 for panel b.

922

923 **Figure 2. Dermal White Adipose Tissue (DWAT) atrophy and increased adipocyte**

924 ***SIX1* expression in SSc a) Hematoxylin and eosin staining of human skin biopsies**

925 from GENISOS cohort participants. **top** Control skin. **middle** early SSc-representative

926 image **bottom** established representative SSc-skin sample. Clinical and demographic  
927 features of biopsies individuals are provided in Supplementary Table 4. Boxes contain  
928 dermal white adipose tissue. Dotted boxes denote DWAT areas. **b)** Representative  
929 images of dual *in situ* hybridization for *SIX1* (teal) and *FABP4* (pink) in 3 SSc and 1  
930 demographically matched control biopsies. Hematoxylin (purple) co-stain labels nuclei. “A”  
931 marks a dermal adnexal structure. Black arrows point to *SIX1* transcript signal. Dash dot  
932 outlines denote the interior periphery of adipocytes. **c)** Representative morphometric  
933 quantification for dual positive FABP4/*SIX1* cells in healthy vs SSc tissue. Significant  
934 levels \*  $P \leq 0.05$  refer to Mann-Whitney comparisons between healthy (N=4) vs SSc  
935 (N=8).

936

937

938 **Figure 3. Dermal white adipose loss precedes fibrosis in the murine model of**  
939 **bleomycin induced skin fibrosis. a)** Schematic representation of SQ bleo model of  
940 skin fibrosis in mice (Created with BioRender) **b)** Representative images of Masson’s  
941 trichrome staining of dorsal mouse skin after 7, 14, 21, and 28 days of SQ vehicle or  
942 bleo treatment. White arrows indicate dermal thickness. Scale bar = 200 $\mu$ m. **c)** Dermal  
943 thickness and **d)** area of DWAT at 7, 14, 21, and 28 days reported in a dot plot  $\pm$ SD of  
944 bleo-injected mice normalized to the average of all vehicle-injected mice at that time  
945 point N=4-5 for each time point. Transcript expression levels for sine oculis homeobox  
946 homolog 1 (*Six1*, **e**), collagen 1a1 (*Col1a1*, **f**), collagen 1a2 (*Col1a2*, **g**), collagen 6a1  
947 (*Col6a1*, **h**), transforming growth factor beta 1 (*Tgfb1*, **i**), serpin family E member 1  
948 (*Serpine1*, **j**) and peroxisome proliferator activated receptor gamma (*Pparg*, **k**) in 7-day

949 skin samples by RT-qPCR. Expression was normalized to 18s rRNA. DWAT = dermal  
950 white adipose tissue. Significance levels \*  $P \leq 0.05$ , \*\*  $P \leq 0.01$ , \*\*\*  $P \leq 0.001$ , and \*\*\*\*  $P$   
951  $\leq 0.0001$  refer to a simple linear regression for panels c-d and an unpaired t-test for  
952 panels e-k. Each individual plot represents a biological N number. N=3-7.

953

954 **Figure 4. Adipocyte *Six1* expression precedes white adipose loss in SQ bleomycin-**  
955 **treated mice.**

956 Representative images of mouse dorsal skin injected with SQ bleo for 7 days (n=6). **a)**  
957 Masson's trichrome staining. **b)** Dual *in situ* hybridization for *Adiponectin* (pink) and  
958 *Six1* (teal). Arrows point to *Six1* signal. DWAT=dermal white adipose tissue. **c)**  
959 Quantification of *Six1* puncta in Adiponectin expressing cells from vehicle (PBS, N=4) or  
960 Bleo treated mice (N=7). **d)** Quantification of *Six1* puncta in smooth muscle actin (SMA)  
961 expressing cells from vehicle (PBS, N=5) or from Bleo (N=4) treated mice. **e)** Dual  
962 immunohistochemistry for SMA (blue signals) and RNAScope for *Six1*, magenta puncta  
963 fibroblasts *f* denote fibroblasts and *v* refer to vessels. Scale bar represents 50 $\mu$ m panel  
964 a, 10 $\mu$ m panel b and 20 $\mu$ m panel e. Significance level \*  $P \leq 0.05$  refers to an un  
965 unpaired t-test for panels c and d.

966

967 **Figure 5. Inducible global deletion of *Six1* inhibits fibrotic gene expression in SQ**  
968 **bleomycin treated mice.**

969 **a)** Schematic representation of experimental design (Created with BioRender).  
970 Following IP tamoxifen administration, iUbc<sup>Cre</sup> and iUbc-*Six1*<sup>-/-</sup> were given 28 days of SQ  
971 vehicle (PBS) or bleo. **b)** Representative dual *Six1* RNAScope (teal) and *adiponectin*

972 (magenta) from bleomycin iUbc<sup>Cre</sup> and iUbcSIX1<sup>-/-</sup> treated mice and **c**) corresponding  
973 *Six1* puncta quantification. Arrows point at *Six1* signals and scale bar represent 20µm.  
974 Transcript expression levels for sine oculis homeobox homolog 1 (*Six1*, **d**), collagen 1a1  
975 (*Col1a1*, **e**), collagen 1a2 (*Col1a2*, **f**), fibronectin (*Fn1*, **g**), elastin (**h**), actin alpha 2  
976 (*Acta2*, **i**), serpin family E member 1 (*Serpine1*, **j**), transforming growth factor beta 1  
977 (*Tgfb1*, **k**), macrophage migration inhibitory factor (*Mif*, **l**), Latent Transforming growth  
978 factor beta binding protein (*Ltbp1*, **m**), (*Ltbp2*, **n**), (*Ltbp3*, **o**), (*Ltbp4*, **p**), *adiponectin* (**q**),  
979 CCAAT enhancer binding protein alpha (*Cebpa*, **r**), peroxisome proliferator activated  
980 receptor gamma (*Pparg*, **s**) at day 28 of bleomycin treatment. Expression was  
981 normalized to 18s rRNA.. Significance levels \* P ≤0.05, \*\* P ≤0.01, \*\*\* P ≤0.001, and  
982 \*\*\*\* P ≤0.0001 refer to an unpaired t-test for panels c-s Each individual plot represents a  
983 biological n number. N=3-8.

984

985 **Figure 6. Global *Six1*-deletion prevents lipolysis and collagen 6 accumulation**

986 **induced by SQ bleomycin a)** Masson's trichrome staining of skin biopsies from  
987 iUbcCre and iUbc-Six1<sup>-/-</sup> mice treated with 28 days of SQ bleo. **b)** High-magnification  
988 Masson's trichrome images of DWAT area marked by square bracket. **c)**  
989 Representative brightfield (left panels) and dual immunofluorescent staining for collagen  
990 6 (yellow signals) and perilipin 1 (red signals) in skin from 28-day bleo-injected iUbc<sup>Cre</sup>  
991 and iUbc-Six1<sup>-/-</sup> mice (right panels). **d)** Quantification of droplet size of perilipin 1-  
992 positive adipocytes in the DWAT. Left: High magnification (100X, zoomed) image of lipid  
993 droplet within DWAT stained with perilipin 1. **e)** Quantification of collagen 6 as percent  
994 positive area in the DWAT. Significance levels \* P ≤0.05 refer to an unpaired t-test.

995 Each individual plot represents a biological N number. N=4-6. V denotes vessels; SM  
996 denotes skeletal muscle. Scale bar represents 200  $\mu\text{m}$  (panel a), 50  $\mu\text{m}$  (panel b), and  
997 20  $\mu\text{m}$  (panel c).

998

999 **Figure 7. Adipocyte SIX1 deletion prevented bleomycin-induced dermal white**

1000 **adipose atrophy and dermal thickness. a)** Representative images of Masson's

1001 trichrome staining from full-thickness skin biopsies. **b)** Quantification of dermal

1002 thickness from Masson's trichrome staining on day 14 of vehicle (PBS) or Bleo SQ

1003 administration from iAdipo<sup>Cre</sup> and iAdipo-Six1<sup>-/-</sup> mice **c)** Representative dual *Six1*

1004 *RNAscope* (teal) and *adiponectin* (magenta) from bleomycin iAdipo<sup>Cre</sup> and iAdipo-SIX1<sup>-/-</sup>

1005 treated mice and **d)** corresponding *Six1* puncta quantification. Arrows point at *Six1*

1006 signals and scale bar represent 20 $\mu\text{m}$ . Transcript expression levels for *Serpine 1* (**e**),

1007 adiponectin (**f**), collagen 1a1 (*Col1a1*, **g**), or collagen 1a2 (*Col1a2*, **h**), from SQ Bleo

1008 treated from iAdipo<sup>Cre</sup> and iAdipo-Six1<sup>-/-</sup> mice on day 14 (panels e, f) or day 28 (panels

1009 g, h). Significance levels \*  $P \leq 0.05$  and \*\*\* $P \leq 0.001$  refer to a One-way ANOVA with a

1010 Bonferroni correction for panel b or un-paired t-test for panels d-h. Each individual plot

1011 represents a biological N number. N=5-13

1012

1013 **Figure 8. Lipid droplets are preserved in bleomycin-treated adipocyte-Six1**

1014 **deficient mice treated with bleomycin. a)** Representative images of

1015 immunofluorescent staining for perilipin 1 in skin from iAdipo<sup>Cre</sup> and iAdipo-Six1<sup>-/-</sup> mice

1016 treated with 14 days of SQ vehicle (PBS) or bleo. Left: brightfield image, Right:

1017 immunofluorescence for perilipin (red signals) images. **b)** Quantification of droplet size

1018 of perilipin-positive adipocytes in the DWAT. Significance levels \*\*  $P \leq 0.01$  and  
1019 \*\*\* $P \leq 0.001$  refer to a Two-way ANOVA with multiple comparison employing a Sidak  
1020 correction for panel b. Each individual plot represents a biological N number V denotes  
1021 vessels; SM denotes skeletal muscle. Scale bar represents  $20\mu\text{m}$ .

1022

1023 **Figure 9. iAdipo<sup>Cre</sup> -Six1 KO mice have decreased collagen 6 deposition in the**

1024 **DWAT after 14 days of SQ bleomycin. a)** Representative images of

1025 immunofluorescent staining for collagen 6 (yellow) in skin samples from iAdipo<sup>Cre</sup> or

1026 iAdipo-Six1<sup>-/-</sup> mice treated with 14 days of SQ bleo. *Left:* Brightfield image and *Right:*

1027 Immunofluorescence for collagen 6 (yellow signals). Area within dotted lines represents

1028 DWAT. **b).** Quantification of collagen 6 as brightness intensity within the DWAT.

1029 Significance levels \*\*\* $P \leq 0.001$  refer to a Two-way ANOVA with multiple comparison

1030 employing a Sidak correction for panel b. Each individual plot represents a biological N

1031 number N=5. **c)** representative dual immunofluorescence for collagen 6 (red signals) or

1032 perilipin (green signals) focusing on the DWAT area of either Bleomycin treated

1033 iAdipo<sup>Cre</sup> (upper panel) iAdipoCreSix1<sup>-/-</sup> mice (lower panel). V denotes vessels; SM

1034 denotes skeletal muscle. Scale bar represents  $20\mu\text{m}$  (panel a) and  $50\mu\text{m}$  (panel b).

1035

1036

1037 **Figure 10. PAI-1 levels are upregulated in bleomycin induced skin fibrosis and**

1038 **track with SIX1 expression levels** (a) protein levels for  $\beta$ -actin, SIX1 and PAI-1, and

1039 from 3T3L1 cells treated with a differentiation cocktail for adipocytes and transfected

1040 with either control plasmic (blue bars, panel b) or CRISPR/Cas9 *Six1* plasmid (green

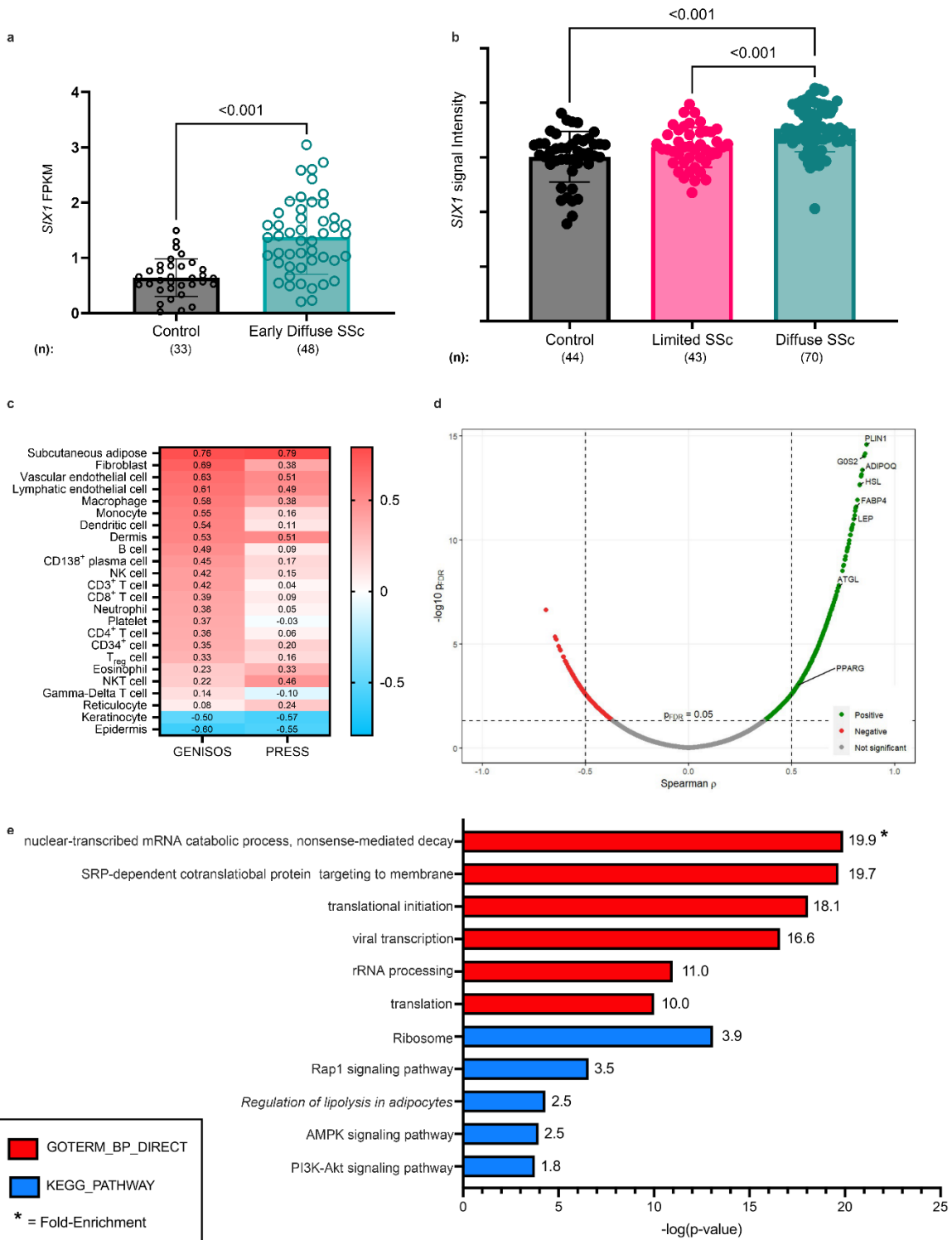
1041 bars, panel a). **b)** *Serpine1* transcript levels and **c)** quantification of PAI-1 signals in  
1042 DWAT from **(d)** IHC for PAI-1 from bleomycin exposed mouse skin for from 2  
1043 independent iAdipoCre or iAdipoSix1<sup>-/-</sup> mice. PAI-1 signals are shown in magenta.  
1044 Significance levels \*\*\*P≤0.001 refer to a Two-way ANOVA with multiple comparison  
1045 employing a Sidak correction for panel b. Significance levels \*P≤0.05 refer to an  
1046 unpaired t-test for panel c. **(e)** Ratios of Gaussian luciferase/secreted embryonic  
1047 alkaline phosphatase (G-Luc/SEAP) showing levels of *SERPINE1*-promoter activity  
1048 from *Six1*OE cells compared with GFP controls at 12 hours. N=3 (panels b and e) and  
1049 N=8 (panel c). Scale bars represent 20μm.  
1050

1051 Table 1. SERPINE1 expression levels in GENISOS and PRESS cohorts  
1052  
1053

<b>Cohort</b>	<b>GENISOS</b>	<b>PRESS</b>
Ensembl_ID	ENSG00000106366.8	
Gene name	SERPINE1	
Gene type	Protein coding	
logFC	1.928211	3.524306
logCPM	2.589225	4.593314
<b>PValue</b>	<b>2.64E-12</b>	<b>4.17E-33</b>
FDR	2.05E-09	9.2E-30
<b>FC</b>	<b>3.805831</b>	<b>11.50593</b>
CPM	6.017755	24.13933
Regulation in SSc group	Up	up

1054  
1055 FC: Fold Change, CPM: Counts per million  
1056  
1057

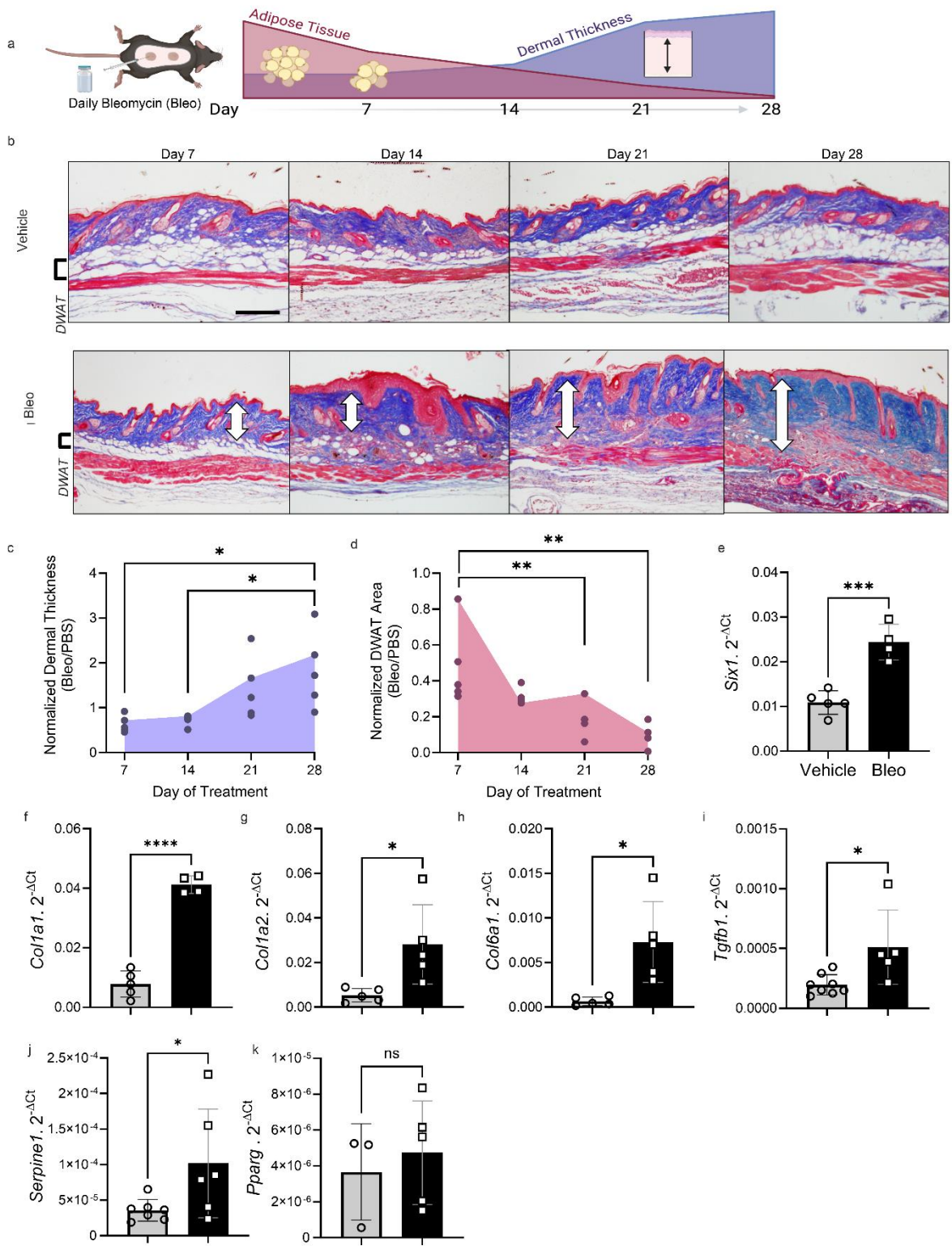
1058 **Figure 1**



1059  
1060  
1061  
1062

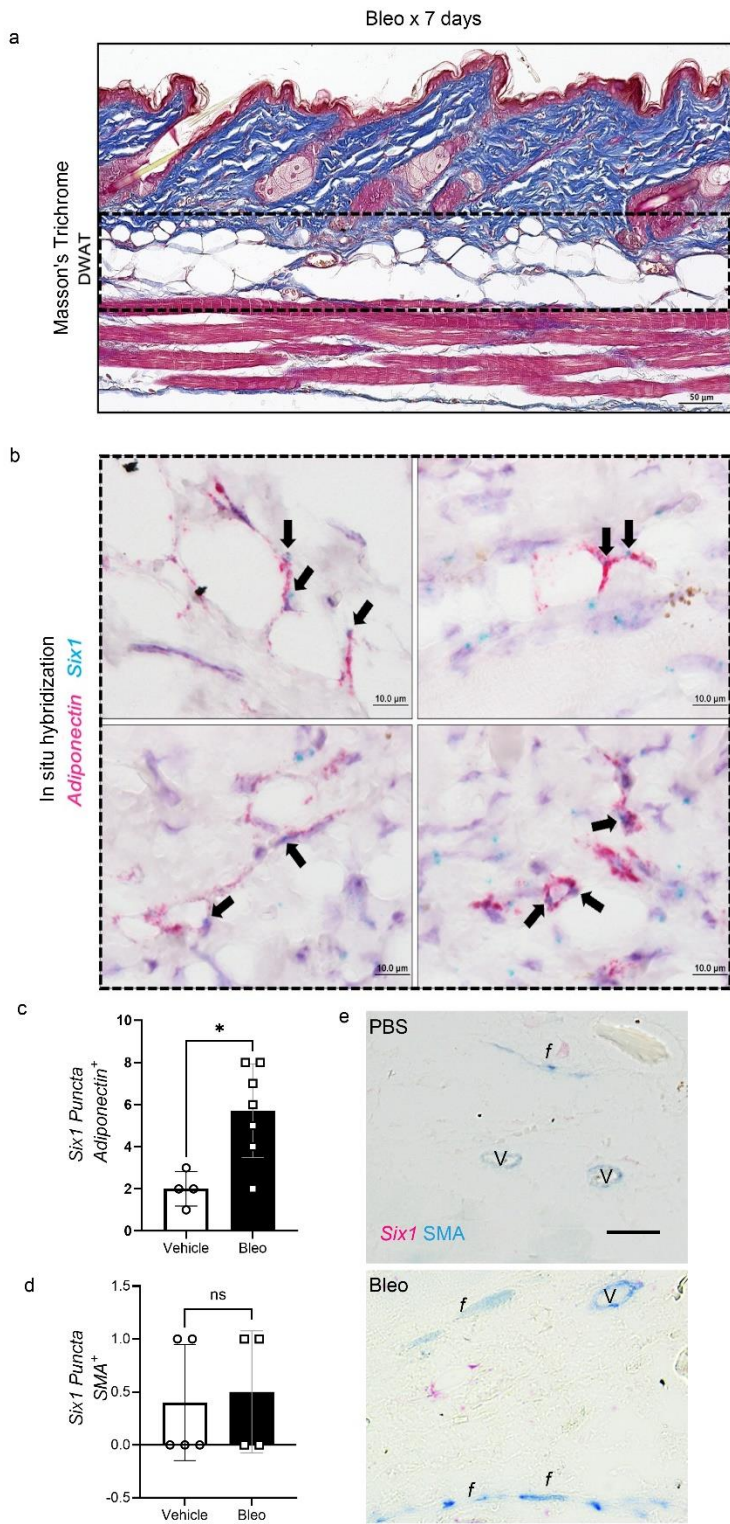


1066 **Figure 3**



1067  
1068  
1069

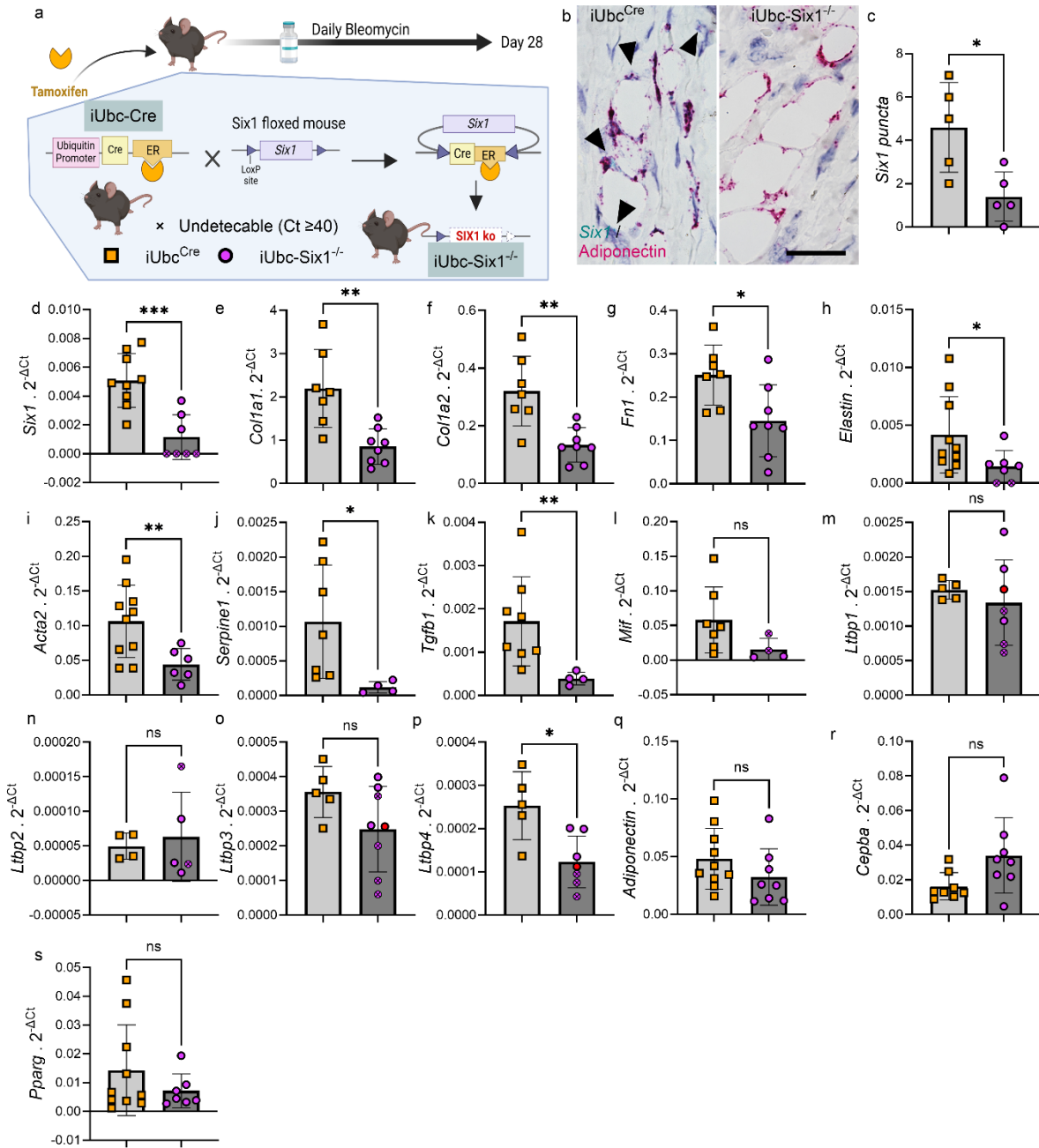
1070 **Figure 4**



1071  
1072  
1073

1074 **Figure 5**

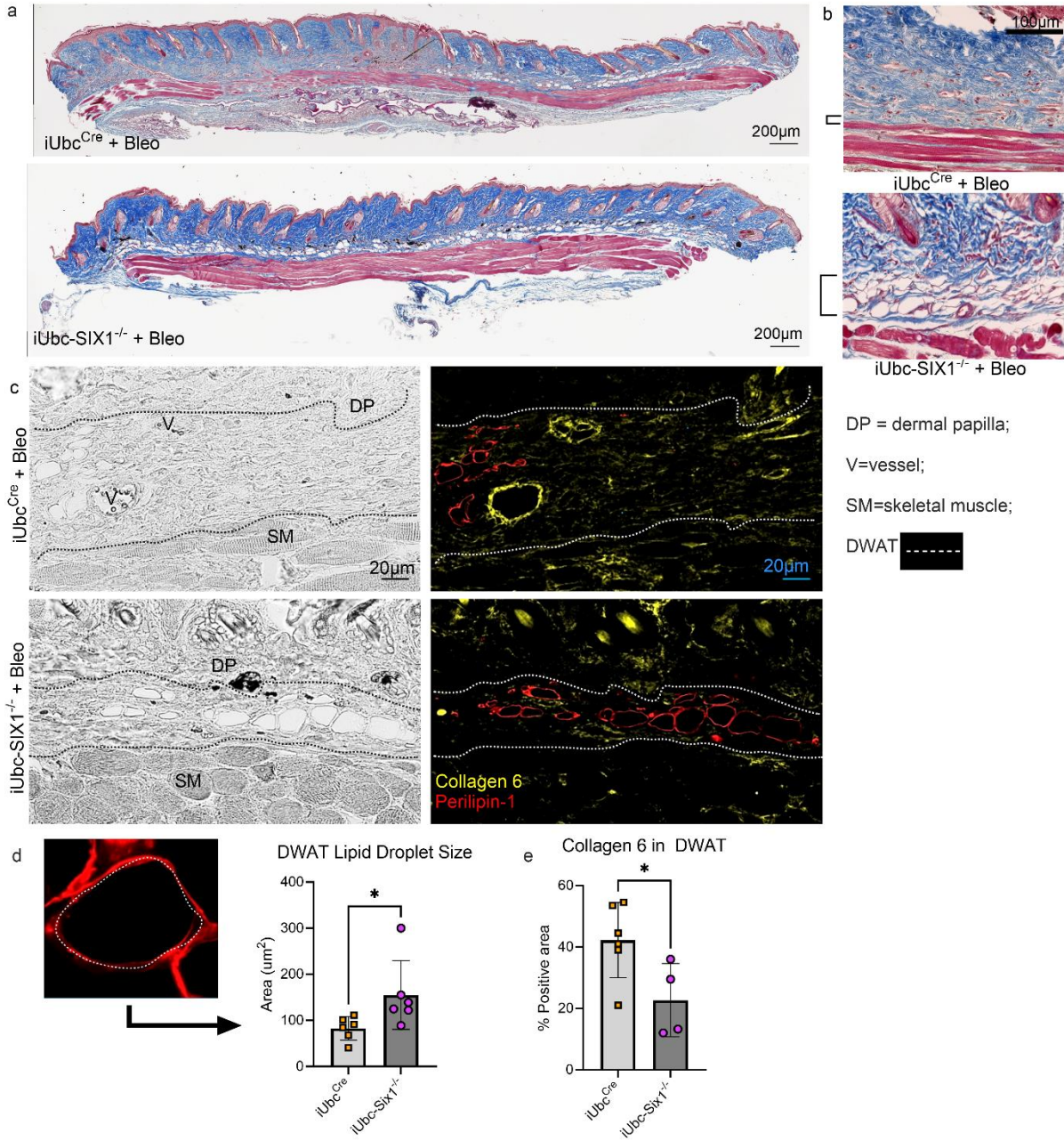
1075  
1076  
1077  
1078



1079  
1080  
1081  
1082  
1083  
1084

1085  
1086  
1087  
1088  
1089

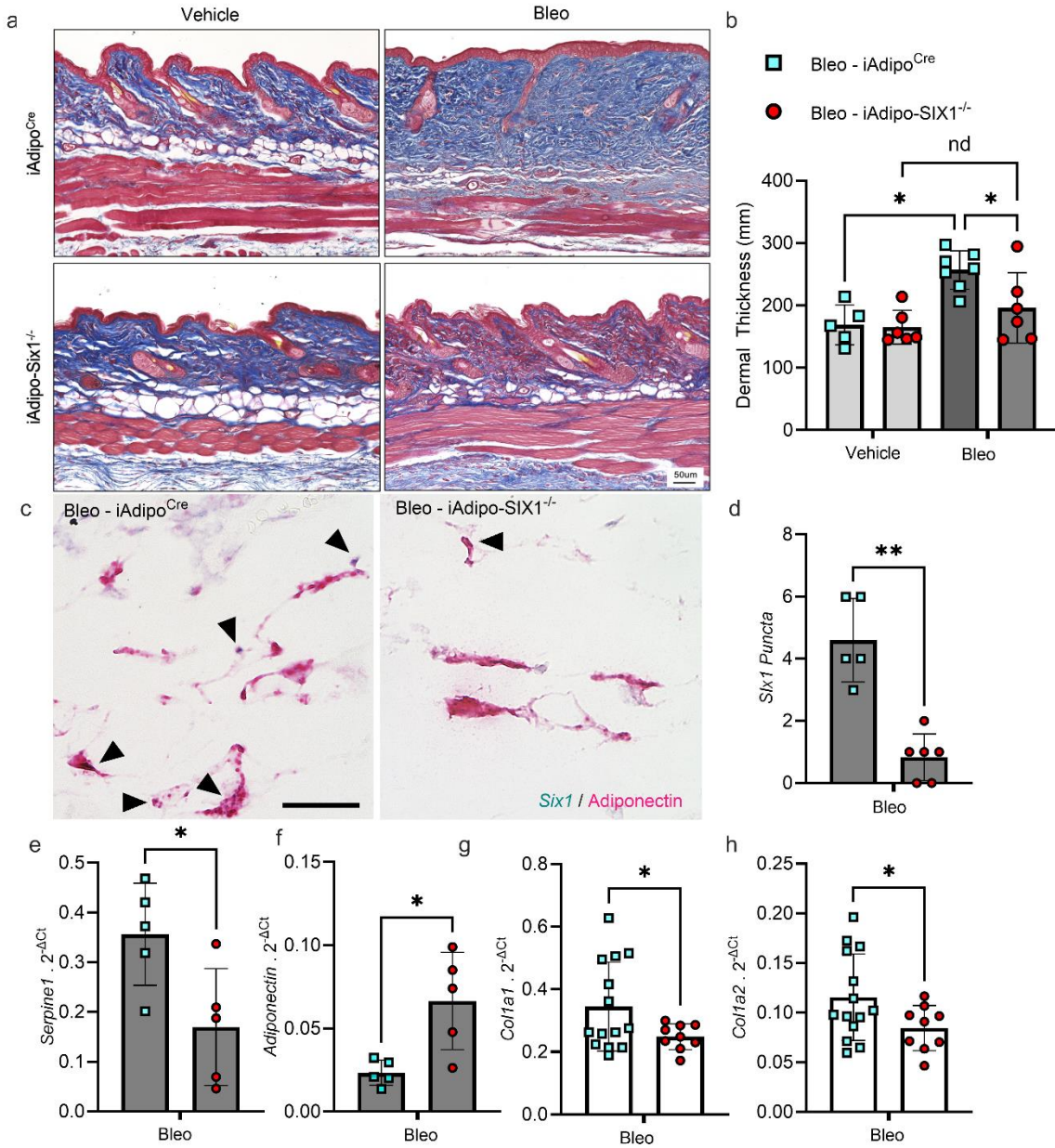
**Figure 6**



1090  
1091  
1092  
1093  
1094

1095  
1096  
1097  
1098

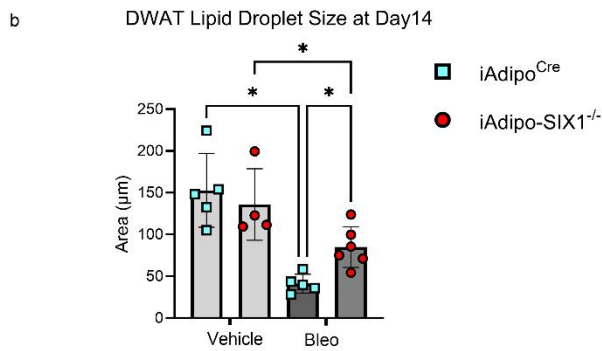
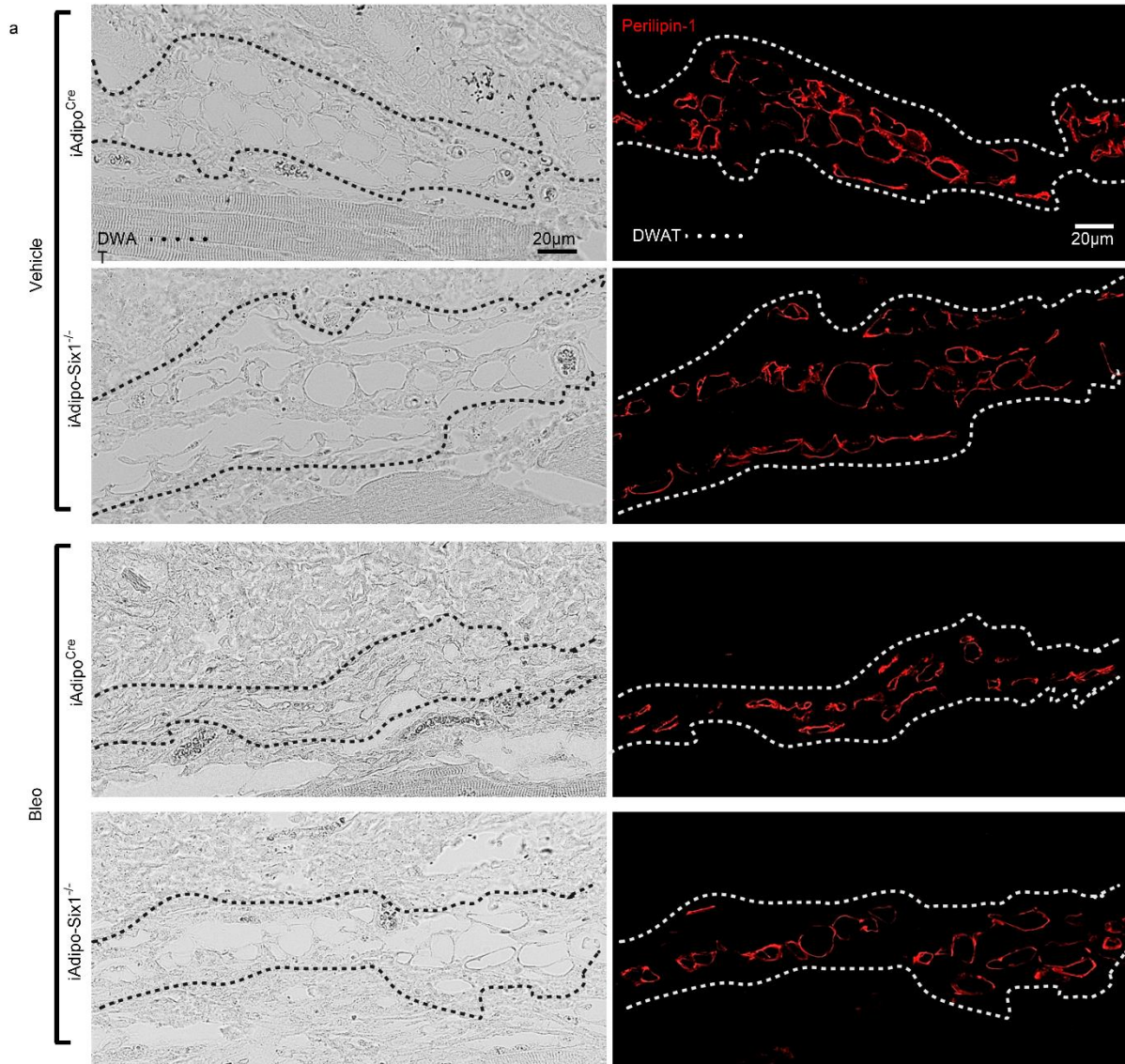
**Figure 7**



1099  
1100  
1101  
1102  
1103  
1104  
1105  
1106

1107  
1108  
1109

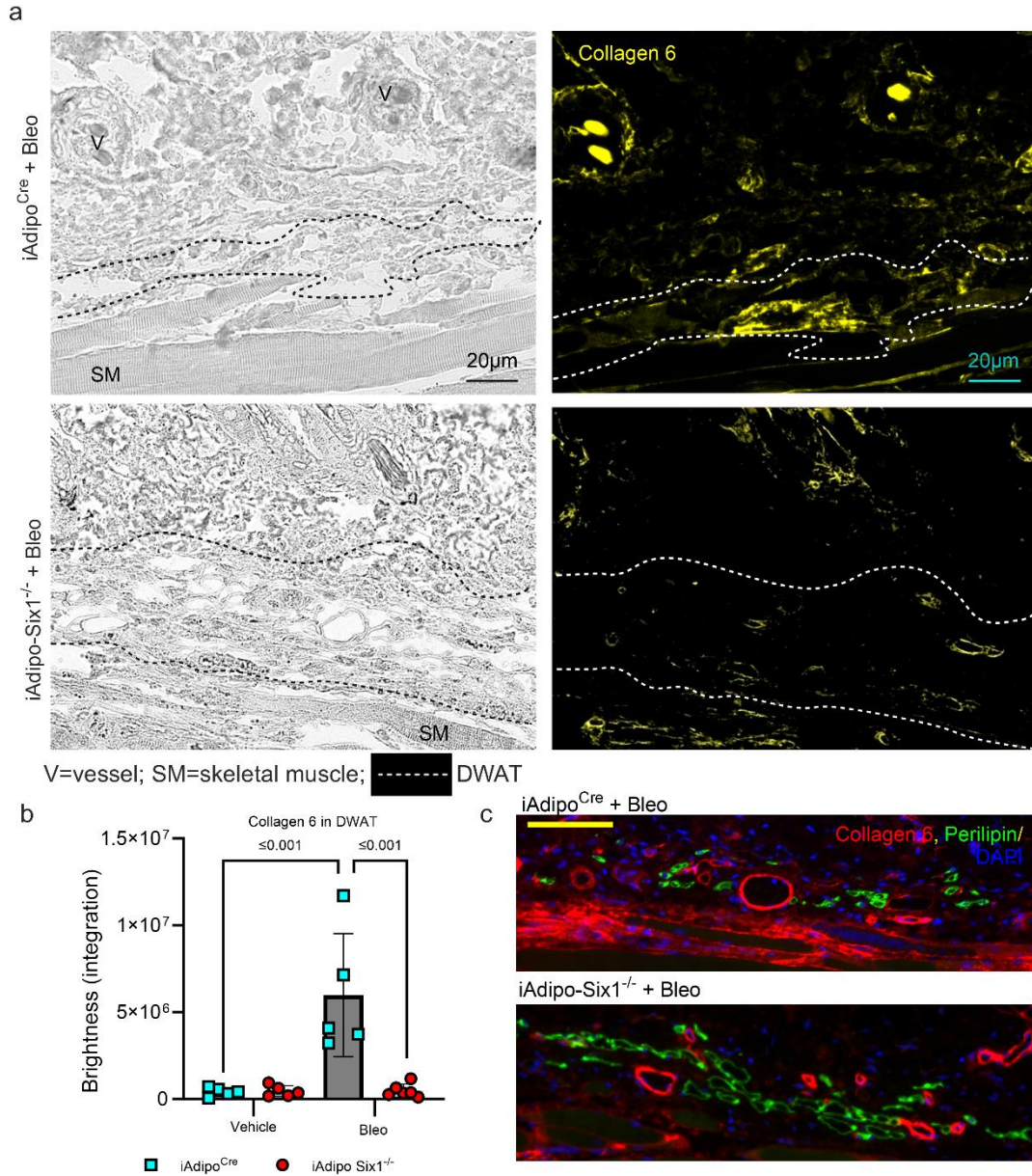
Figure 8



1110  
1111

1112  
1113  
1114  
1115  
1116

**Figure 9**



1117  
1118  
1119  
1120  
1121  
1122  
1123  
1124

